Australian Government
Department of Defence
Science and Technology

Magnetic signatures of spherical bodies in Earth's magnetic field — a comparison of analytical and finite element analysis solutions

Ryan Michael Thomas

Maritime Division
Defence Science and Technology Group

DST-Group–TR–3530

ABSTRACT

Calculating magnetic signatures using analytical techniques becomes infeasible for complex geometries such as submarines, hence numerical techniques, such as finite element analysis, must be used instead. In this report we compare analytical and finite element solutions utilising COMSOL for calculating the magnetic induction of a permeable spherical shell with an internal current band in uniform magnetic induction. The analytical and finite element analysis solutions were found to be approximately equal, this verifies that modelling of magnetic signatures of submarines using COMSOL will generate correct data.

RELEASE LIMITATION

Approved for Public Release

Produced by

Maritime Division
Locked Bag 7005,
Liverpool, NSW 1871, Australia

Telephone: 1300 333 362

September, 2018

AR-017-281

APPROVED FOR PUBLIC RELEASE

Magnetic signatures of spherical bodies in Earth's magnetic field — a comparison of analytical and finite element analysis solutions

Executive Summary

In this report we compare analytical and finite element solutions to validate the use of COMSOL software for calculating the magnetic signature of permeable materials with current bands in background magnetic fields.

The analytical techniques used for determining the magnetic signature of a simple shape, such as a spherical shell, cannot be used to calculate the magnetic signature of a submarine due to its complex structure. Instead, the magnetic signature of a submarine must be numerically calculated using finite element analysis. However, finite element analysis introduces both discretisation and numerical errors. This report quantifies these errors.

The magnetic signature is calculated for the following domains:

- a permeable spherical shell in uniform magnetic induction B_0
- a permeable spherical shell with an internal current band
- a permeable spherical shell with an internal current band in uniform magnetic induction B_0.

The finite element solutions were found to closely approximate the analytical solutions. These solutions may be used to study the *induced* magnetic signatures of ferromagnetic bodies and coils found on modern submarines.

COMSOL may be used to calculate the magnetic induction of permeable materials with internal current bands in background magnetic fields.

This page is intentionally blank

Author

Ryan Michael Thomas
MD

Ryan Michael Thomas received a Bachelor of Science (First Class Honours) (Physics, Computer Science) from the University of Sydney. He has been working for DST Group since 2018 in Magnetic Signatures and Electromagnetic Engineering with a focus on the Future Submarine Program.

This page is intentionally blank

Contents

Figures

1. Introduction

A comparison between analytical and finite element solutions has been conducted to validate the use of COMSOL software for calculating the magnetic induction of permeable materials in background magnetic fields with current bands. Calculating magnetic induction using analytical techniques becomes infeasible for complex geometries, instead numerical techniques such as finite element analysis must be used.

The analytical solution of a permeable spherical shell with an internal current band in uniform magnetic induction B_0 is given in [1], [2]. A comparison between the analytical and finite element solution of a permeable spherical shell with an *external* current band is given in [3]. This report compares the analytical to finite element analysis solutions of a permeable spherical shell with an *internal* current band in background magnetic induction B_0.

Calculation of the magnetic induction using the analytical method requires solving Laplace's, or Poisson's, equation with boundary conditions, this is outlined in Section 2. The analytical solution consists of a series expansion of associated Legendre functions. For simple geometries solving Laplace's equation is feasible. However, for complex geometries the number of boundary conditions and the complexity of the solution renders analytical solutions infeasible, and hence numerical techniques must be used instead. Finite element analysis, which is outlined in Section 3, is a numerical method which may be used for calculating magnetic potential and hence magnetic induction. Finite element analysis converts a second order partial differential equation into a system of linear equations by discretising the spatial domain. However, discretising the spatial domain may introduce discretisation error, which will result in a numerical solution unequal to the analytical solution. This paper quantifies the error created when using finite element analysis for calculating magnetic signatures for three domains:

- a permeable spherical shell in uniform magnetic induction B_0
- a permeable spherical shell with an *internal* current band
- a permeable spherical shell with an *internal* current band in uniform magnetic induction B_0.

Magnetic induction signatures, their absolute value comparisons, and errors are presented. These solutions may be used to study the interaction of ferromagnetic bodies and coils found on modern submarines.

2. Background of magnetostatics

2.1. Magnetic scalar potential

The basic equations of magnetostatics are [4]:

$$\nabla \cdot \mathbf{B} = 0 \tag{1}$$
$$\nabla \times \mathbf{H} = \mathbf{J} \tag{2}$$

where $\mathbf{B}$ is the magnetic induction, $\mathbf{H}$ is the magnetic field, and $\mathbf{J}$ is the current. If there are no free currents, i.e. $\mathbf{J} = 0$, this means $\nabla \times \mathbf{H} = 0$ and we can introduce a scalar potential Φ_M:

$$\mathbf{H} = -\nabla \Phi_M \tag{3}$$

Note that $\mathbf{H} = -\nabla \Phi_M$ is analogous to $\mathbf{E} = -\nabla \Phi_E$ in electrostatics. If the medium is linear:

$$\mathbf{B} = -\mu \nabla \Phi_M \tag{4}$$
$$\nabla \cdot \mathbf{B} = \nabla \cdot (-\mu \nabla \Phi_M) = 0 \tag{5}$$

where μ is the magnetic permeability of the material. If μ is piecewise constant then the magnetic scalar potential satisfies the Laplace equation:

$$\nabla^2 \Phi_M = 0 \tag{6}$$

2.2. Laplace's equation and associated Legendre functions

Laplace's equation in spherical coordinates is given by [5]:

$$\nabla^2 \Phi_M = \frac{1}{r^2}\frac{\partial}{\partial r}\left(r^2 \frac{\partial \Phi_M}{\partial r}\right) + \frac{1}{r^2 \sin\theta}\frac{\partial}{\partial \theta}\left(\sin\theta \frac{\partial \Phi_M}{\partial \theta}\right) + \frac{1}{r^2 \sin^2\theta}\frac{\partial^2 \Phi_M}{\partial \phi^2} = 0 \tag{7}$$

where r is radial distance, θ is the azimuthal angle, ϕ is the polar angle. Separating variables:

$$\Phi_M = U(r)\Theta(\theta)\Omega(\phi) \tag{8}$$

Substituting into equation (7) and multiplying by $\frac{r^2 \sin^2\theta}{U\Theta\Omega}$:

$$r^2 \sin^2\theta \left(\frac{1}{U}\frac{d^2 U}{dr^2} + \frac{1}{\Theta r^2 \sin\theta}\frac{d}{d\theta}\left(\sin\theta \frac{d\Theta}{d\theta}\right)\right) + \frac{1}{\Omega}\frac{d^2\Omega}{d\phi^2} = 0 \tag{9}$$

This gives three equations where m and $n(n+1)$ are constants:

$$-m^2 = \frac{1}{\Omega}\frac{d^2\Omega}{d\phi^2} \tag{10a}$$
$$0 = \frac{1}{\sin\theta}\frac{d}{d\theta}\left(\sin\theta\frac{d\Theta}{d\theta}\right) + \left(n(n+1) - \frac{m^2}{\sin^2\theta}\right)\Theta \tag{10b}$$
$$0 = \frac{1}{r^2}\frac{d}{dr}\left(r^2\frac{dU}{dr}\right) - \frac{n(n+1)}{r^2}U \tag{10c}$$

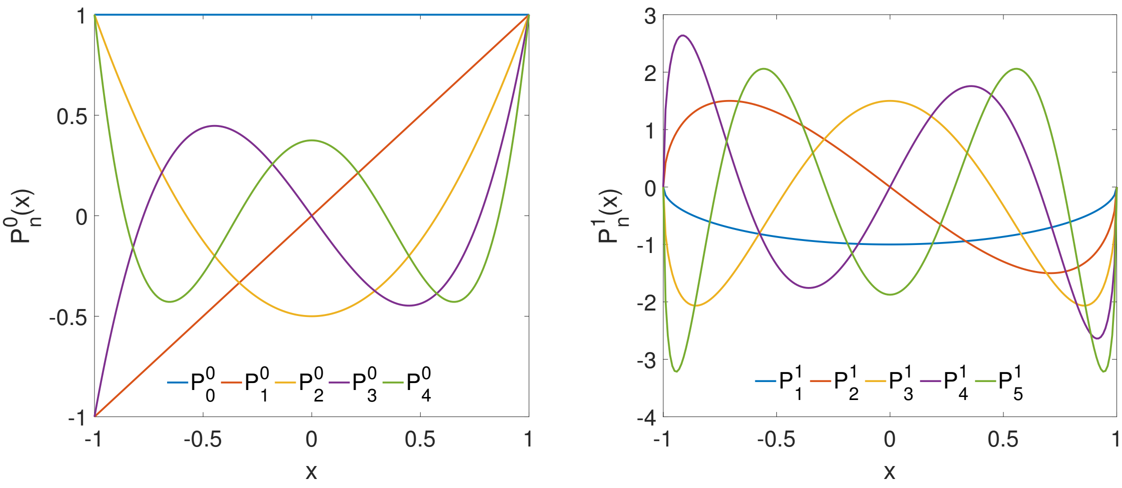

(i) $P_n^0(x)$ *(ii)* $P_n^1(x)$

Figure 1: Associated Legendre functions of the first kind.

The solutions of these equations are [6]:

$$\Omega = A_{nm} \cos m\phi + B_{nm} \sin m\phi \tag{11a}$$

$$\Theta = C_{nm} P_n^m(\cos\theta) \tag{11b}$$

$$U = \frac{D_{nm}}{r^{n+1}} + E_{nm} r^n \tag{11c}$$

where A_{nm},B_{nm},C_{nm},D_{nm}, and E_{nm} are constants, and $P_n^m(x)$ are associated Legendre functions of the first kind. The magnetic scalar potential is given by [5]:

$$\Phi_M(r,\theta,\phi) = \sum_{n=0}^{\infty}\sum_{m=0}^{n}(A_{nm}\cos m\phi + B_{nm}\sin m\phi)C_{nm}P_n^m(\cos\theta)\left(\frac{D_{nm}}{r^{n+1}} + E_{nm}r^n\right) \tag{12}$$

The associated Legendre functions of the first kind for real argument x are given by [7]:

$$P_n^m(x) = (-1)^m(1-x^2)^{m/2}\frac{d^m}{dx^m}P_n(x) \tag{13}$$

where $P_n(x)$ is the Legendre polynomial and may be expressed using Rodrigues' formula:

$$P_n(x) = \frac{1}{2^n n!}\frac{d^n}{dx^n}(x^2-1)^n \tag{14}$$

$P_n^m(x)$ are bounded in the interval $-1 \leq x \leq 1$. A plot of the $P_n^0(x)$ and $P_n^1(x)$ associated Legendre functions of the first kind are given in Figure 1.

3. Background of finite element analysis

3.1. Second-order partial differential equation

This section will focus on finite element analysis in two dimensions. Finite element analysis solves the generic second-order partial differential equation given by [8]:

$$\frac{\partial}{\partial x}\left(\alpha_x \frac{\partial u}{\partial x}\right) + \frac{\partial}{\partial y}\left(\alpha_y \frac{\partial u}{\partial y}\right) + \beta u = g \tag{15}$$

where α_x, α_y, β, and g are constants and u is the variable for which the equation is solved. Laplace's equation is a special case of equation (15) given by:

$$\frac{\partial^2 \Phi}{\partial x^2} + \frac{\partial^2 \Phi}{\partial y^2} = 0 \tag{16}$$

where $u = \Phi$, $\alpha_x = \alpha_y = 1$, $\beta = 0$, and $g = 0$. Similarly, Poisson's equation is a special case of equation (15) given by:

$$\frac{\partial}{\partial x}\left(\epsilon \frac{\partial \Phi}{\partial x}\right) + \frac{\partial}{\partial y}\left(\epsilon \frac{\partial \Phi}{\partial y}\right) = -\rho_v \tag{17}$$

where $u = \Phi$, $\alpha_x = \alpha_y = \epsilon$, $\beta = 0$, and $g = -\rho_v$. Hence, finite element analysis may be used to numerically solve electromagnetics problems, such as a permeable material in a uniform magnetic field, or the magnetic field of a current band in a permeable spherical shell.

3.2. Discretisation of the domain

Consider the irregular shape given in Figure 2i. To use finite element analysis to determine electromagnetic properties such as magnetic induction, the domain must be discretised into finite elements. The most common shapes used are triangles such as those given in 2ii. Large triangles give a large discretisation error, which may be improved by using small triangles in areas with large variations. Once the domain has been meshed with finite elements the interpolation functions must be developed for the triangles.

3.3. Interpolation functions

An interpolation function is used to determine the potential inside the triangular finite elements given in Figure 2ii. The potential u inside the interior of a triangle finite element, as given in Figure 3, is calculated as:

$$u = u_1^e N_1 + u_2^e N_2 + u_3^e N_3 \tag{18}$$

where u_1^e, u_2^e, and u_3^e are the potentials at the vertices of the triangle, and N_1, N_2, and N_3 are the interpolation functions. The interpolation functions must be continuous within the finite element and at least once differentiable, hence the simplest choice is a *polynomial of degree one*.

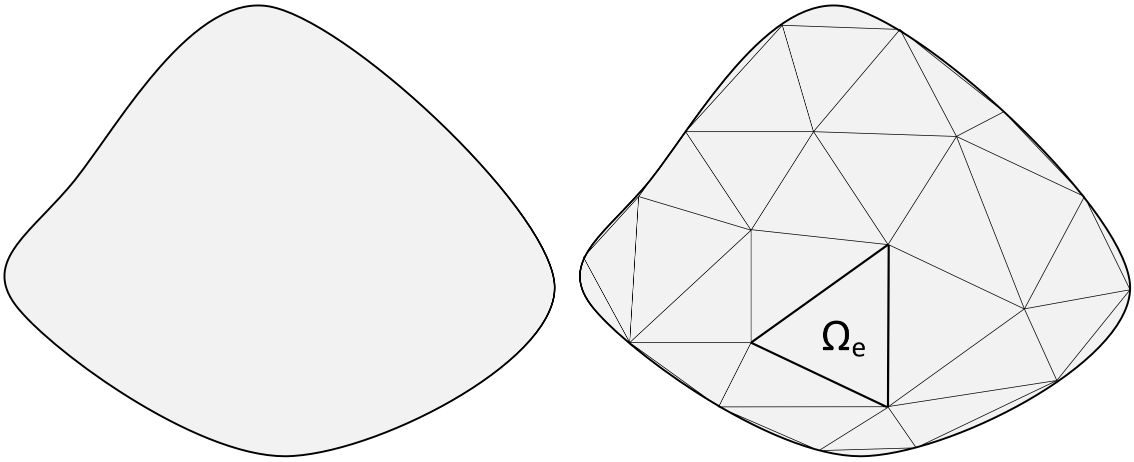

(i) Irregular 2-D domain *(ii) Discretised 2-D domain*

Figure 2: Triangular finite elements are used to discretise the irregular 2-D domain. Ω_e represents the area of the triangle finite element.

3.4. The method of weighted residual

A weak formulation, where equation (15) is no longer required to be exact, may be obtained by introducing a weighted residual element given by [8]:

$$r^e = \frac{\partial}{\partial x}\left(\alpha_x \frac{\partial u}{\partial x}\right) + \frac{\partial}{\partial y}\left(\alpha_y \frac{\partial u}{\partial y}\right) + \beta u - g \tag{19}$$

where r^e is the residual element. If the numerical solution is equal to the analytical solution then the residual element should equal zero. However, as the domain has been discretised this is not the case. The objective, then, of finite element analysis is to minimise the residual element by multiplying r^e with a weight function w, integrating over the area of the element Ω^e and setting the integral to zero:

$$\int\int_{\Omega^e} w\left[\frac{\partial}{\partial x}\left(\alpha_x \frac{\partial u}{\partial x}\right) + \frac{\partial}{\partial y}\left(\alpha_y \frac{\partial u}{\partial y}\right) + \beta u - g\right] dxdy = 0 \tag{20}$$

Introducing the identity:

$$w\frac{\partial}{\partial x}\left(\alpha_x \frac{\partial u}{\partial x}\right) = \frac{\partial}{\partial x}\left(w\alpha_x \frac{\partial u}{\partial x}\right) - \alpha_x \frac{\partial w}{\partial x}\frac{\partial u}{\partial x} \tag{21}$$

Substituting this identity into equation (20) gives:

$$\begin{aligned}\int\int_{\Omega^e} &\left[\frac{\partial}{\partial x}\left(w\alpha_x \frac{\partial u}{\partial x}\right) + \frac{\partial}{\partial y}\left(w\alpha_y \frac{\partial u}{\partial y}\right)\right] dxdy \\ &- \int\int_{\Omega^e}\left[\alpha_x \frac{\partial w}{\partial x}\frac{\partial u}{\partial x} + \alpha_y \frac{\partial w}{\partial y}\frac{\partial u}{\partial y}\right] dxdy + \int\int_{\Omega^e} \beta w u \; dxdy = \int\int_{\Omega^e} wg \; dxdy\end{aligned} \tag{22}$$

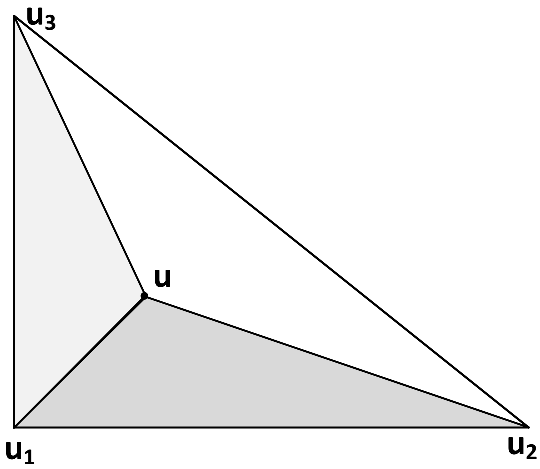

Figure 3: A triangular finite element with nodes 1, 2, and 3. The potential u is found by interpolation of u_1, u_2, and u_3.

Green's theorem states that the area integral of the divergence of a vector equals the total outward flux through the contour that bounds the area:

$$\int\int_{\Omega^e} (\nabla_t \cdot \mathbf{A}) dA = \oint_{\Gamma^e} \mathbf{A} \cdot \hat{a_n} dl \tag{23}$$

where $\mathbf{A}$ is the vector quantity of interest, Γ^e is the boundary of the element, and $\hat{a_n}$ is the outward unit vector that is normal to the boundary of the element. Applying Green's theorem to the first integral of equation (22), and defining the normal unit vector as $\hat{a_n} = \hat{a_x} n_x + \hat{a_y} n_y$, the weak form of the differential equation becomes:

$$\begin{aligned} -\int\int_{\Omega^e} \left[\alpha_x \frac{\partial w}{\partial x}\frac{\partial u}{\partial x} + \alpha_y \frac{\partial w}{\partial y}\frac{\partial u}{\partial y} \right] dxdy + \int\int_{\Omega^e} \beta w u \; dxdy \\ = \int\int_{\Omega^e} w g \; dxdy - \oint_{\Gamma^e} w \left(\alpha_x \frac{\partial u}{\partial x} n_x + \alpha_y \frac{\partial u}{\partial y} n_y \right) dl \end{aligned} \tag{24}$$

The weight function is $w = N_i$ for i=1,2,...n which means the weak form of the differential is discretised given by:

$$\begin{aligned} -\int\int_{\Omega^e} \left[\alpha_x \frac{\partial N_i}{\partial x} \sum_{j=1}^{n} u_j^e \frac{\partial N_j}{\partial x} + \alpha_y \frac{\partial N_i}{\partial y} \sum_{j=1}^{n} u_j^e \frac{\partial N_j}{\partial y} \right] dxdy + \int\int_{\Omega^e} \beta N_i \left(\sum_{j=1}^{n} u_j^e N_j \right) dxdy \\ = \int\int_{\Omega^e} N_i g \; dxdy - \oint_{\Gamma^e} N_i \left(\alpha_x \frac{\partial u}{\partial x} n_x + \alpha_y \frac{\partial u}{\partial y} n_y \right) dl \qquad \text{for} \qquad i = 1, 2, ..., n \end{aligned} \tag{25}$$

The second-order partial differential equation has now been converted into a system of linear equations:

$$\begin{bmatrix} K_{11}^e & K_{12}^e & \cdots & K_{1n}^e \\ K_{21}^e & K_{22}^e & \cdots & K_{2n}^e \\ \vdots & \vdots & \ddots & \vdots \\ K_{n1}^e & K_{n2}^e & \cdots & K_{nn}^e \end{bmatrix} \begin{bmatrix} u_1^e \\ u_2^e \\ \vdots \\ u_n^e \end{bmatrix} = \begin{bmatrix} b_1^e \\ b_2^e \\ \vdots \\ b_n^e \end{bmatrix} \tag{26}$$

where:

$$K_{ij}^e = M_{ij}^e + T_{ij}^e \tag{27a}$$

$$b_i^e = f_i^e + p_i^e \tag{27b}$$

$$M_{ij}^e = -\int\int_{\Omega^e} \left[\alpha_x \frac{\partial N_i}{\partial x}\frac{\partial N_j}{\partial x} + \alpha_y \frac{\partial N_i}{\partial y}\frac{\partial N_j}{\partial y} \right] dxdy \tag{27c}$$

$$T_{ij}^e = \int\int_{\Omega^e} \beta N_i N_j \; dxdy \tag{27d}$$

$$f_i^e = \int\int_{\Omega^e} N_i g \; dxdy \tag{27e}$$

$$p_i^e = -\oint_{\Gamma^e} N_i \left(\alpha_x \frac{\partial u}{\partial x} n_x + \alpha_y \frac{\partial u}{\partial y} n_y \right) dl \tag{27f}$$

3.5. Boundary conditions

Equation (26) is singular, and thus does not have a unique solution. Imposing boundary conditions allows calculation of a unique solution. A Dirichlet boundary condition, which specifies the values a numerical solution must adhere to on the boundary of the domain, reduces the size of the final linear system by the number of finite elements minus the number of boundary conditions. Consider the boundary condition $u_1^e = u_b^e$. To implement this boundary condition the first line associated with the boundary condition is eliminated and $u_1^e = u_b^e$ is substituted in all the remaining $N - 1$ equations given by:

$$\begin{bmatrix} K_{22}^e & K_{23}^e & \cdots & K_{2n}^e \\ K_{32}^e & K_{33}^e & \cdots & K_{3n}^e \\ \vdots & \vdots & \ddots & \vdots \\ K_{n2}^e & K_{n3}^e & \cdots & K_{nn}^e \end{bmatrix} \begin{bmatrix} u_2^e \\ u_3^e \\ \vdots \\ u_n^e \end{bmatrix} = \begin{bmatrix} b_2^e - K_{21} u_b \\ b_3^e - K_{31} u_b \\ \vdots \\ b_n^e - K_{n1} u_b \end{bmatrix} \tag{28}$$

Solving equation (28) for u gives the potential, such as scalar magnetic potential, for all finite elements.

To summarise, we started with a domain in which we wanted to calculate the magnetic field or magnetic induction described by Laplace's or Poisson's equation. These may be solved numerically by using the finite element analysis method. First the domain was discretised into triangle elements, then the second order partial differential equations were converted into a system of linear equations with boundary conditions. These linear equations are solved for u, the magnetic potential.

4. Magnetic induction of a permeable spherical shell in uniform magnetic induction B_0

Consider the spherical shell of permeable material in uniform magnetic induction $\mathbf{B} = B_0\hat{\mathbf{z}}$ given in Figure 4.

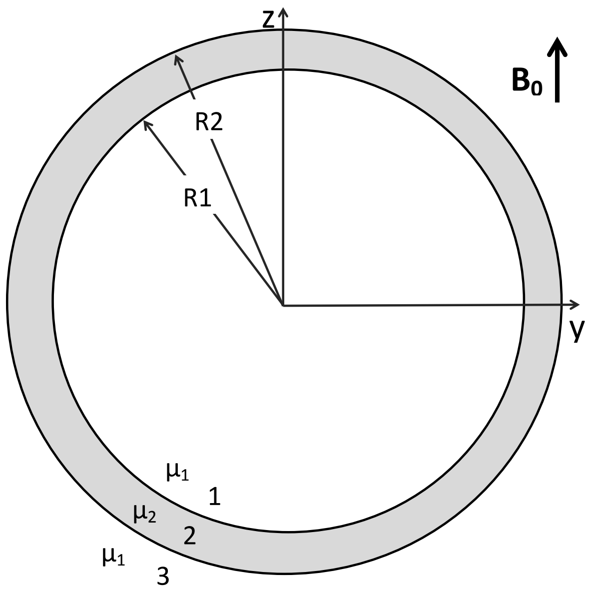

Figure 4: Spherical shell in uniform magnetic induction B_0 where R_1 is the inner radius, R_2 is the outer radius, μ_1 and μ_2 are permeabilities, and 1, 2, 3 refers to the regions considered.

4.1. Analytical solution

The potential due to the external field is $\Phi_M{=}{-}H_0 r\cos\theta$ where H_0 is the background magnetic field. The potential in the three regions is given by [5]:

$$\Phi_1 = \sum_{n=0}^{\infty} A_n r^n P_n(\cos\theta) \qquad \text{region 1} \qquad (29a)$$

$$\Phi_2 = \sum_{n=0}^{\infty} \left(B_n r^n + \frac{C_n}{r^{n+1}}\right) P_n(\cos\theta) \qquad \text{region 2} \qquad (29b)$$

$$\Phi_3 = -H_0 r\cos\theta + \sum_{n=0}^{\infty} \frac{D_n}{r^{n+1}} P_n(\cos\theta) \qquad \text{region 3} \qquad (29c)$$

where A_n, B_n, C_n, and D_n are constants. The solutions in different regions are connected by the boundary conditions [9]:

$$\mathbf{H_j} \cdot \mathbf{n} = \frac{\mu_i}{\mu_j} \mathbf{H_i} \cdot \mathbf{n} \tag{30a}$$

$$\mathbf{H_j} \times \mathbf{n} = \mathbf{H_i} \times \mathbf{n} \tag{30b}$$

where $\mathbf{H_i}$ is the magnetic field in region i, $\mathbf{H_j}$ is the magnetic field in region j, μ_i is the magnetic permeability in region i, μ_j is the magnetic permeability in region j, and $\mathbf{n}$ is a vector normal to the boundary. Boundary conditions, H_θ and B_r, must be continuous at $r = R_1$ and $r = R_2$.

$$\frac{\partial \Phi_1}{\partial \theta} = \frac{\partial \Phi_2}{\partial \theta} \tag{31a}$$

$$\mu_1 \frac{\partial \Phi_1}{\partial r} = \mu_2 \frac{\partial \Phi_2}{\partial r} \tag{31b}$$

$$\frac{\partial \Phi_2}{\partial \theta} = \frac{\partial \Phi_3}{\partial \theta} \tag{31c}$$

$$\mu_1 \frac{\partial \Phi_2}{\partial r} = \mu_2 \frac{\partial \Phi_3}{\partial r} \tag{31d}$$

For Φ_3 we have Earth's constant field term $-H_0 r \cos\theta$. As this is equated to $P_n(\cos\theta)$, only $n = 1$ is allowed (i.e. $P_1(\cos\theta) = \cos\theta$), and all other n terms are equal to zero, giving:

$$\Phi_1 = Ar\cos\theta \tag{32a}$$

$$\Phi_2 = \left[Br + \frac{C}{r^2}\right]\cos\theta \tag{32b}$$

$$\Phi_3 = -H_0 r\cos\theta + \frac{D}{r^2}\cos\theta \tag{32c}$$

Solving by applying the boundary conditions gives the D coefficient:

$$D = \left[\frac{(2\mu' + 1)(\mu' - 1)}{(2\mu' + 1)(\mu' + 2) - 2\frac{R_1^3}{R_2^3}(\mu' - 1)^2}\right](R_2^3 - R_1^3)H_0 \tag{33}$$

where $\mu' = \mu_2/\mu_1$. The magnetic field vector is given by:

$$\mathbf{H} = -\nabla\Phi_M = -\left[\frac{\partial \Phi_M}{\partial r}\hat{\mathbf{r}} + \frac{1}{r}\frac{\partial \Phi_M}{\partial \theta}\hat{\boldsymbol{\theta}} + \frac{1}{r\sin\theta}\frac{\partial \Phi_M}{\partial \phi}\hat{\boldsymbol{\phi}}\right] \tag{34}$$

In region 3 the magnetic field is given by:

$$\mathbf{H_3} = \left[H_0\cos\theta + \frac{2D}{r^3}\cos\theta\right]\hat{\mathbf{r}} + \left[-H_0\sin\theta + \frac{D}{r^3}\sin\theta\right]\hat{\boldsymbol{\theta}} \tag{35}$$

with spherical vector components:

$$H_r = H_0\cos\theta + \frac{2D}{r^3}\cos\theta \tag{36a}$$

$$H_\theta = -H_0\sin\theta + \frac{D}{r^3}\sin\theta \tag{36b}$$

$$H_\phi = 0 \tag{36c}$$

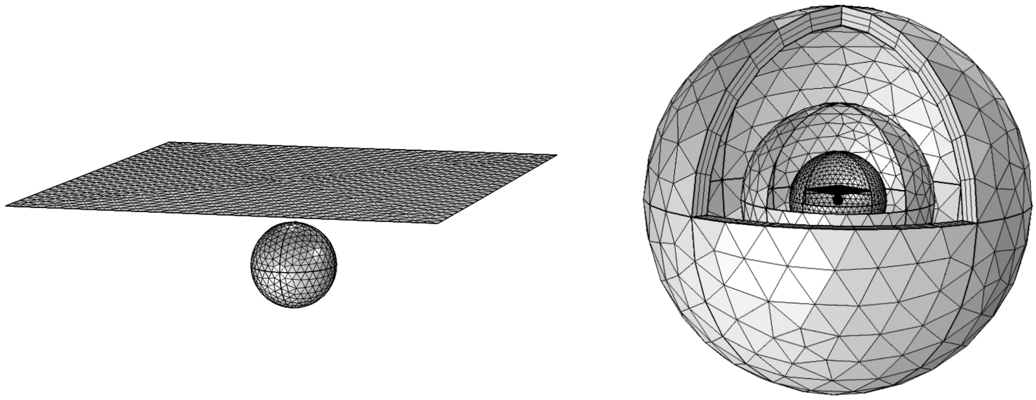

(i) Mesh of spherical shell and plane. *(ii) 3D mesh construction.*

Figure 5: Finite element analysis model created in COMSOL of a permeable spherical shell in uniform magnetic induction B_0.

The spherical to rectangular vector transformations are given by:

$$H_x = H_r \sin\theta \cos\phi + H_\theta \cos\theta \cos\phi - H_\phi \sin\phi \tag{37a}$$

$$H_y = H_r \sin\theta \sin\phi + H_\theta \cos\theta \sin\phi + H_\phi \cos\phi \tag{37b}$$

$$H_z = H_r \cos\theta - H_\theta \sin\theta \tag{37c}$$

The magnetic induction in region 3 is (using $B = \mu H$):

$$B_x = \frac{3Dxz}{\mu_1(x^2+y^2+z^2)^{5/2}} \tag{38a}$$

$$B_y = \frac{3Dyz}{\mu_1(x^2+y^2+z^2)^{5/2}} \tag{38b}$$

$$B_z = B_0 + \frac{D(2z^2-x^2-y^2)}{\mu_1(x^2+y^2+z^2)^{5/2}} \tag{38c}$$

4.2. Finite element analysis solution

The finite element analysis model was created using COMSOL version 5.3 [10] and the AC/DC Module [11]. The model contains a spherical shell of permeable material at its centre. The inner surface of the spherical shell was meshed and the interior of the shell was swept with a mesh of three layers. A plane at $x = 20$m, which is the plane used throughout this paper, was finely meshed to ensure accurate results during post processing. The mesh of these two domains is given in Figure 5i. Three concentric shells were created to slowly expand from a very fine mesh near the permeable shell to a coarse mesh at the boundary. As COMSOL uses a finite volume, and in reality magnetic fields extend to infinity, the infinite elements option in COMSOL was applied to the outer concentric shell. The mesh of concentric shells are given in Figure 5ii and encompasses the plane and spherical shell. Finally, a uniform magnetic field was applied outside of the permeable spherical shell.

4.3. Comparison between analytical and finite element analysis solutions

A plot of the magnetic induction B_x, B_y, B_z, and B_{total} in region 3 for a spherical shell in uniform magnetic induction $\mathbf{B_0}$ is given in Figures 6, 7, 8, and 9 respectively. The analytical and finite element analysis solutions are approximately equal. B_y was calculated at $y = 10$m due to the magnetic signature being zero at $y = 0$m. The root-mean-squared errors are $B_x = 0.17$nT, $B_y = 0.07$nT, $B_z = 0.21$nT, and $B_{total} = 0.23$nT.

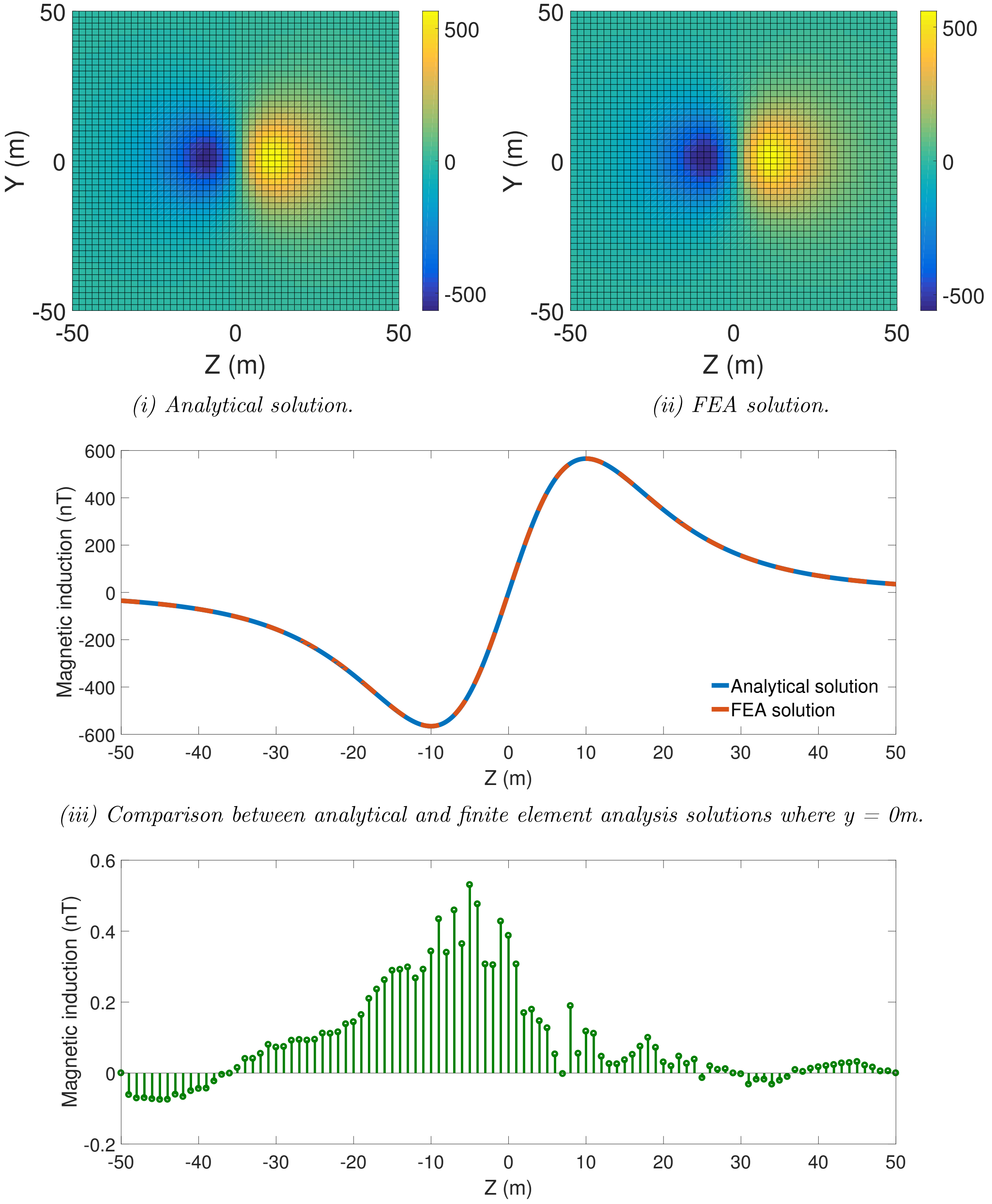

(i) Analytical solution.

(ii) FEA solution.

(iii) Comparison between analytical and finite element analysis solutions where $y = 0m$.

(iv) Error between analytical and finite element analysis solutions where $y = 0m$.

Figure 6: Magnetic induction B_x (nT) of a spherical shell in uniform magnetic induction B_0 in the y-z plane where $x = 20m$, $R_1 = 9.98m$, $R_2 = 10m$, $B_0 = 55\ 000nT$, $\mu_1 = 4\pi{\times}10^{-7}Hm^{-1}$, and $\mu_2/\mu_1 = 80$.

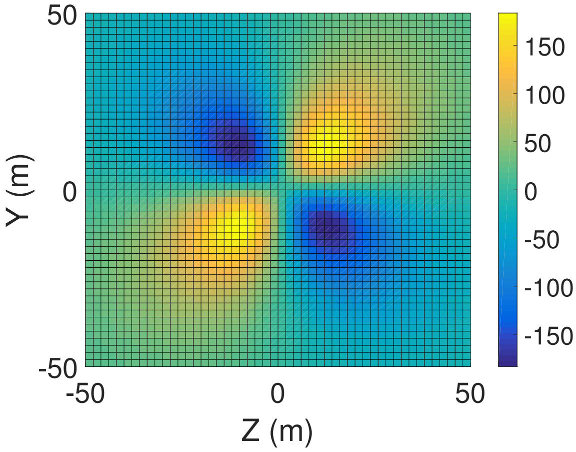

(i) Analytical solution.

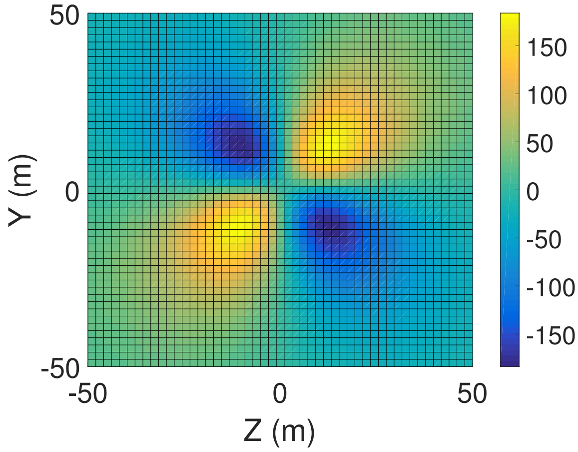

(ii) FEA solution.

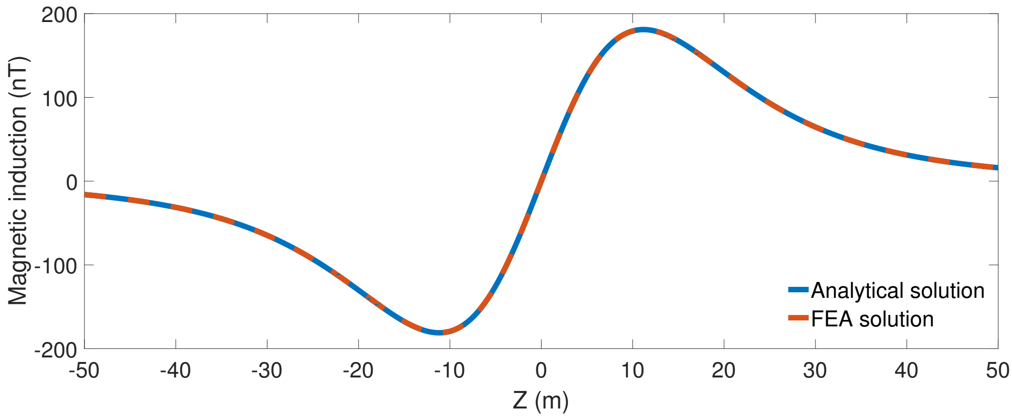

(iii) Comparison between analytical and finite element analysis solutions where y = 10m.

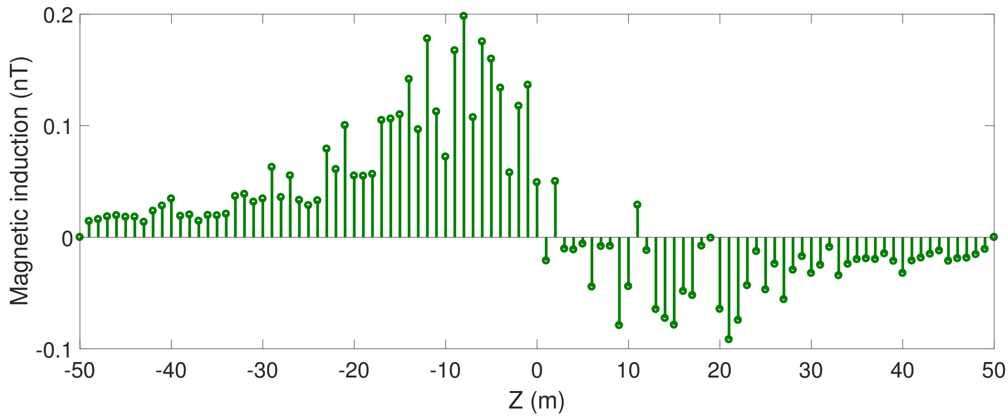

(iv) Error between analytical and finite element analysis solutions where y = 10m.

Figure 7: Magnetic induction B_y (nT) of a spherical shell in uniform magnetic induction B_0 in the y-z plane where $x = 20m$, $R_1 = 9.98m$, $R_2 = 10m$, $B_0 = 55\ 000nT$, $\mu_1 = 4\pi\times10^{-7}Hm^{-1}$, and $\mu_2/\mu_1 = 80$.

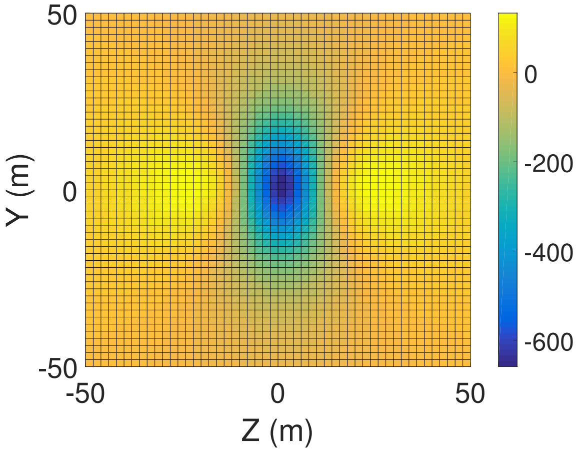

(i) Analytical solution.

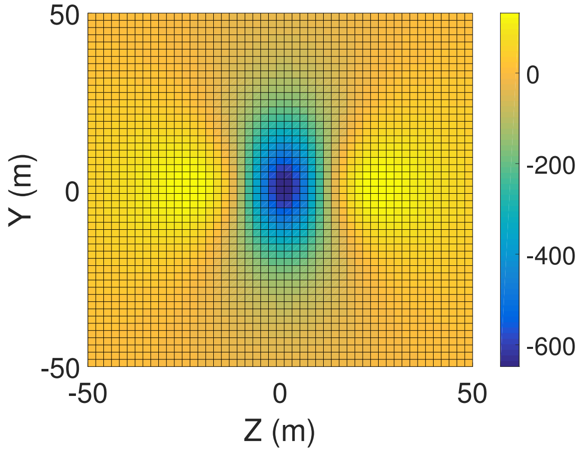

(ii) FEA solution.

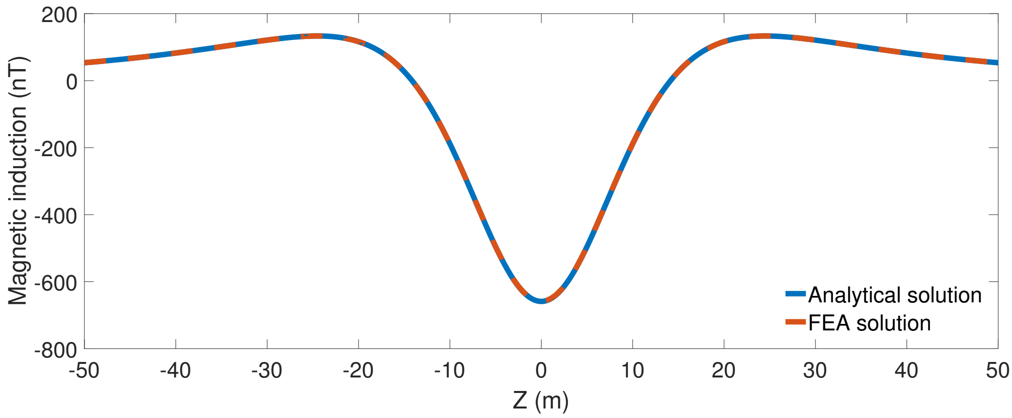

(iii) Comparison between analytical and finite element analysis solutions where $y = 0m$.

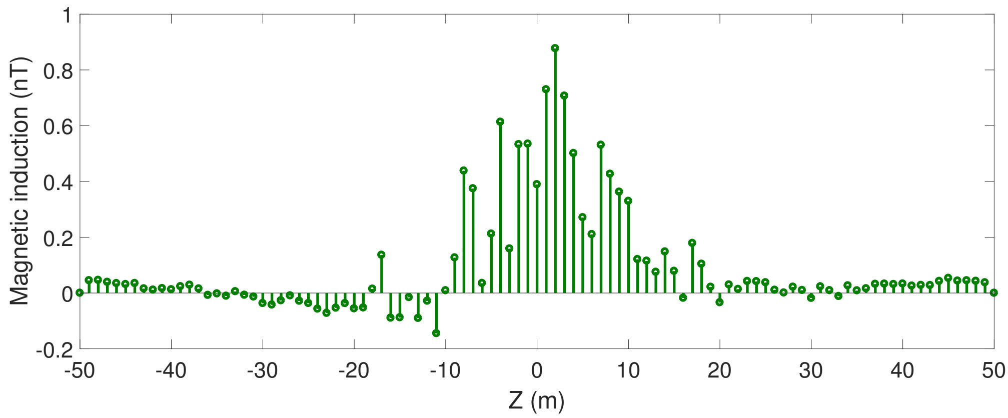

(iv) Error between analytical and finite element analysis solutions where $y = 0m$.

Figure 8: Magnetic induction B_z (nT) of a spherical shell in uniform magnetic induction B_0 in the y-z plane where $x = 20m$, $R_1 = 9.98m$, $R_2 = 10m$, $B_0 = 55\ 000nT$, $\mu_1 = 4\pi \times 10^{-7} Hm^{-1}$, and $\mu_2/\mu_1 = 80$.

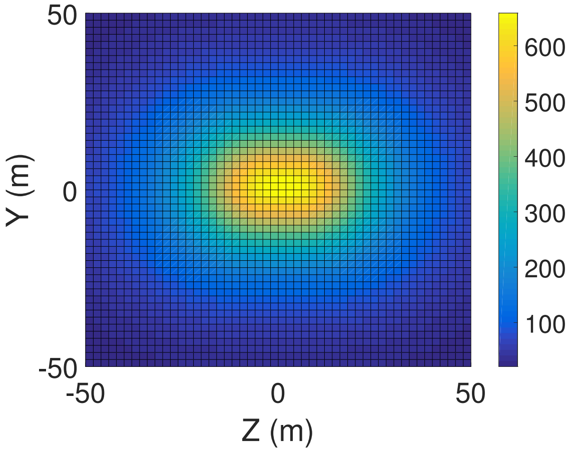

(i) Analytical solution.

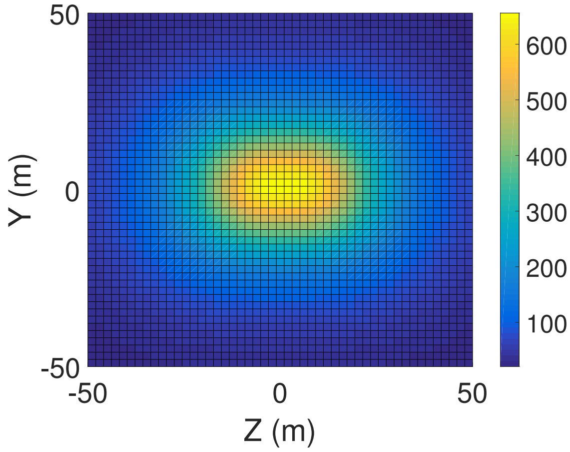

(ii) FEA solution.

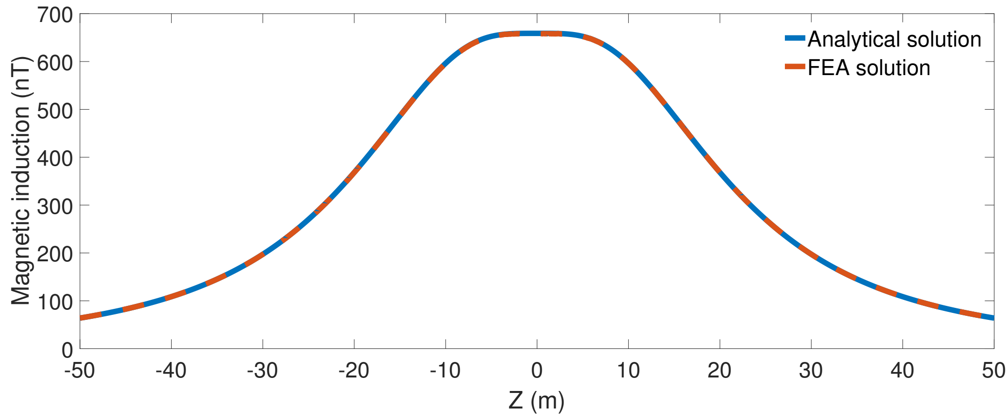

(iii) Comparison between analytical and finite element analysis solutions where $y = 0m$.

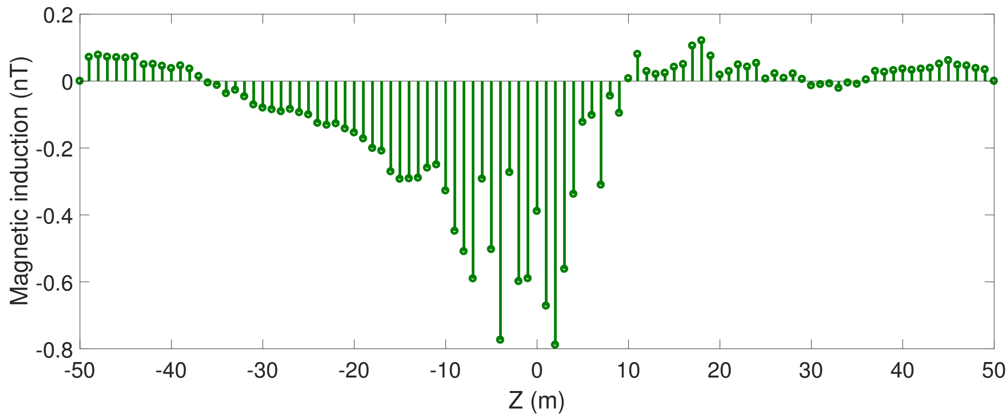

(iv) Error between analytical and finite element analysis solutions where $y = 0m$.

Figure 9: Magnetic induction B_{total} (nT) of a spherical shell in uniform magnetic induction B_0 in the y-z plane where $x = 20m$, $R_1 = 9.98m$, $R_2 = 10m$, $B_0 = 55\ 000nT$, $\mu_1 = 4\pi \times 10^{-7} Hm^{-1}$, and $\mu_2/\mu_1 = 80$.

5. Magnetic induction of a permeable spherical shell with an internal current band

Consider the spherical shell with an internal current band in Figure 10.

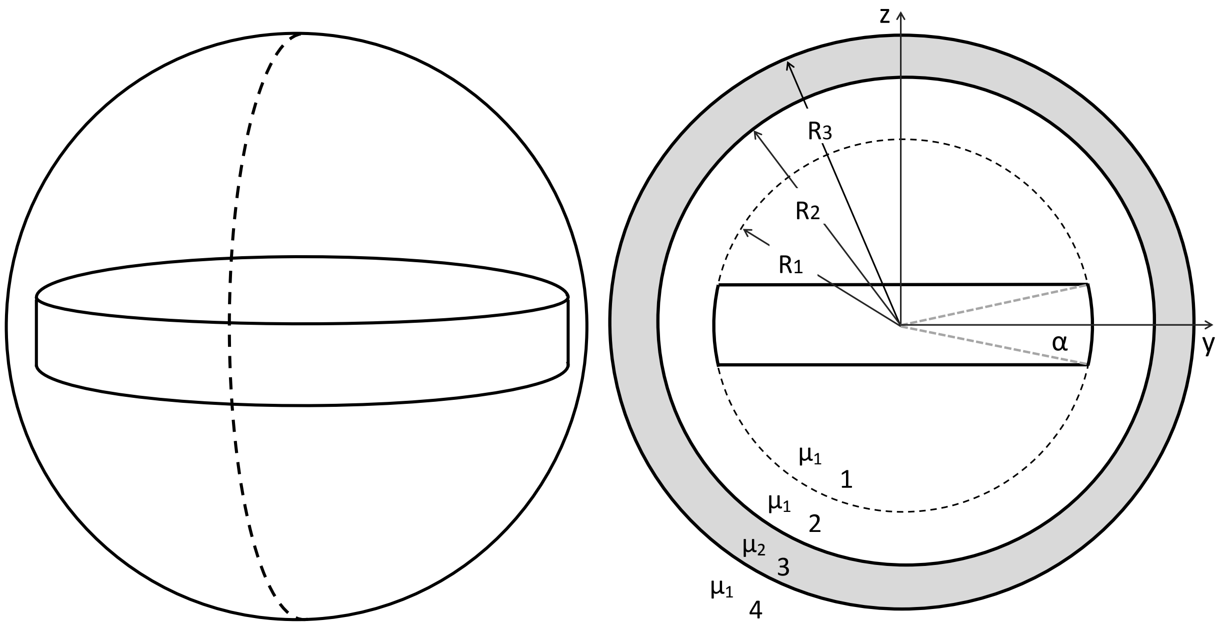

(i) Schematic diagram.

(ii) Cross section of the schematic.

Figure 10: Spherical shell with an internal current band where R_1 is the current band radius, R_2 is the inner shell radius, R_3 is the outer shell radius, μ_1 and μ_2 are permeabilities, α is the angle of the current band considered from the centre of the spherical shell, and 1, 2, 3, and 4 are the regions considered.

5.1. Analytical solution

The magnetic induction may be expressed as [1], [5]:

$$\mathbf{B} = \nabla \times \mathbf{A} \tag{39}$$

where $\mathbf{A}$ is the magnetostatic vector potential. Using the constitutive relationship $\mathbf{B} = \mu\mathbf{H}$ and equation (2) then:

$$\frac{1}{\mu}\nabla \times (\nabla \times \mathbf{A}) = \mathbf{J} \tag{40}$$

where $\mathbf{J}$ is the current vector. Using the identity $\nabla \times (\nabla \times \mathbf{F}) = \nabla(\nabla \cdot \mathbf{F}) - \nabla^2\mathbf{F}$:

$$\frac{1}{\mu}(\nabla(\nabla \cdot \mathbf{A}) - \nabla^2\mathbf{A}) = \mathbf{J} \tag{41}$$

Using the Coulomb gauge $\nabla \cdot \mathbf{A} = 0$ we get Poisson's equation:

$$\nabla^2\mathbf{A} = -\mu\mathbf{J} \tag{42}$$

If $\mathbf{J} = 0$, Poisson's equation reduces to Laplace's equation. The boundary conditions which must be satisfied are:

$$\mathbf{n_{ij}} \cdot (\mu_j \mathbf{H_j} - \mu_i \mathbf{H_i}) = 0 \tag{43a}$$

$$\mathbf{n_{ij}} \times \left(\frac{\mathbf{B_j}}{\mu_j} - \frac{\mathbf{B_i}}{\mu_i} \right) = \mathbf{J_S} \tag{43b}$$

where $\mathbf{J_S}$ is the surface current density. The spherical symmetry of the surface current density implies that the vector potential has only an azimuthal component and is given by Poisson's equation [1], [4]:

$$\frac{\partial^2 A_\phi}{\partial r^2} + \frac{2}{r}\frac{\partial A_\phi}{\partial r} + \frac{1}{r^2}\frac{\partial^2 A_\phi}{\partial \theta^2} + \frac{\cot\theta}{r^2}\frac{\partial A_\phi}{\partial \theta} + \frac{1}{r^2 \sin^2\theta}\frac{\partial^2 A_\phi}{\partial \phi^2} = -\mu J_\phi(r,\theta) \tag{44}$$

Using separation of variables the general solution of the vector potential can be expressed as:

$$A_\phi = \sum_{n=1}^{\infty} \left(A_n r^n + \frac{B_n}{r^{n+1}} \right) P_n^1(\cos\theta) \tag{45}$$

The magnetic induction is given by:

$$\mathbf{B} = \nabla \times \mathbf{A} = \frac{\hat{r}}{r\sin\theta}\left(\frac{\partial}{\partial\theta}(A_\phi \sin\theta) - \frac{\partial A_\theta}{\partial \phi} \right) + \frac{\hat{\theta}}{r}\left(\frac{1}{\sin\theta}\frac{\partial A_r}{\partial\phi} - \frac{\partial}{\partial r}(rA_\phi) \right) + \frac{\hat{\phi}}{r}\left(\frac{\partial}{\partial r}(rA_\theta) - \frac{\partial A_r}{\partial \theta} \right) \tag{46}$$

Only the A_ϕ component is relevant in this example and therefore the magnetic induction is given by:

$$B_r = \frac{1}{r\sin\theta}\frac{\partial}{\partial\theta}(\sin\theta A_\phi) \tag{47a}$$

$$B_\theta = -\frac{1}{r}\frac{\partial}{\partial r}(rA_\phi) \tag{47b}$$

$$B_\phi = 0 \tag{47c}$$

The current may be expanded in associated Legendre functions:

$$J_\phi(r,\theta) = J\sum_{n=1}^{\infty} K_n P_n^1(\cos\theta) \tag{48}$$

where the constant K_n is given by using the orthogonality relation:

$$K_n = \frac{2n+1}{2n(n+1)} \int_0^\pi P_n^1(\cos\theta)\sin\theta d\theta \tag{49}$$

If the current is symmetrical around the x-y plane then K_n may be expressed as:

$$K_n = \frac{2n+1}{2n(n+1)} \left[\int_{\pi/2-\alpha}^{\pi/2} P_n^1(\cos\theta)\sin\theta d\theta + \int_{\pi/2}^{\pi/2+\alpha} P_n^1(\cos\theta)\sin\theta d\theta \right] \tag{50}$$

The magnetic potential in the four regions are given by:

$$A_{\phi 1} = \sum_{n=1}^{\infty} (A_n r^n)\, P_n^1(\cos\theta) \tag{51a}$$

$$A_{\phi 2} = \sum_{n=1}^{\infty} \left(B_n r^n + \frac{C_n}{r^{n+1}} \right) P_n^1(\cos\theta) \tag{51b}$$

$$A_{\phi 3} = \sum_{n=1}^{\infty} \left(D_n r^n + \frac{E_n}{r^{n+1}} \right) P_n^1(\cos\theta) \tag{51c}$$

$$A_{\phi 4} = \sum_{n=1}^{\infty} \left(\frac{F_n}{r^{n+1}} \right) P_n^1(\cos\theta) \tag{51d}$$

where A_n, B_n, C_n, D_n, E_n, and F_n are constants. Applying boundary conditions and solving the simultaneous equations gives:

$$J_n(\theta) = J_n \tag{52a}$$

$$J'_n = \frac{\mu_1 J K_n R_1^{n+2}}{2n+1} \tag{52b}$$

$$X = \frac{-R_3^{2n+1}\left[1 + \left(\frac{n+1}{n}\frac{\mu_1}{\mu_2}\right)\right]}{1 - \frac{\mu_1}{\mu_2}} \tag{52c}$$

$$D_n = \frac{\frac{1}{\mu_1} J'_n (2n+1) R_2^{-(n+2)}}{\frac{1}{\mu_1}(n+1)R_2^{n-1} + \frac{1}{\mu_1} X(n+1) R_2^{-(n+2)} - \frac{1}{\mu_2}(n+1)R_2^{n-1} + \frac{1}{\mu_2} n X R_2^{-(n+2)}} \tag{52d}$$

$$C_n = J'_n \tag{52e}$$

$$E_n = D_n X \tag{52f}$$

$$B_n = -J'_n R_2^{-(2n+1)} + D_n + E_n R_2^{-(2n+1)} \tag{52g}$$

$$A_n = B_n + C_n R_1^{-(2n+1)} \tag{52h}$$

$$F_n = D_n R_3^{2n+1} + E_n \tag{52i}$$

The magnetic induction in region 4 is given by:

$$B_r = \frac{1}{r\sin\theta} \sum_{n=1}^{\infty} \frac{F_n}{r^{n+1}} \frac{\partial}{\partial\theta}(\sin\theta P_n^1(\cos\theta)) \tag{53a}$$

$$B_\theta = \frac{1}{r} \sum_{n=1}^{\infty} F_n P_n^1(\cos\theta) \frac{n}{r^{n+1}} \tag{53b}$$

$$B_\phi = 0 \tag{53c}$$

The spherical to rectangular vector transformations are given by:

$$B_x = B_r \sin\theta\cos\phi + B_\theta\cos\theta\cos\phi - B_\phi\sin\phi \tag{54a}$$
$$B_y = B_r \sin\theta\sin\phi + B_\theta\cos\theta\sin\phi + B_\phi\cos\phi \tag{54b}$$
$$B_z = B_r \cos\theta - B_\theta\sin\theta \tag{54c}$$

5.2. Finite element analysis solution

The finite element analysis model was created using COMSOL version 5.3 [10] using the AC/DC Module [11]. The current band was created by removing lower and upper portions of an infinitesimally thin spherical sheet as given in Figure 11i. The current band was then meshed as given in Figure 11ii. The model has a spherical shell of permeable material at its centre. The inner surface of the spherical shell was meshed and the interior of the shell was swept with a mesh of three layers as given in Figures 11iii and 11iv. A plane at $x = 20$m was finely meshed to ensure accurate results during post processing. Then three concentric shells were created to slowly converge from a very fine mesh near the permeable shell to a coarse mesh at the boundary. As COMSOL uses a finite volume, and in reality magnetic fields extend to infinity, the infinite elements option in COMSOL was applied to the outer concentric shell.

5.3. Comparison between analytical and finite element analysis solutions

A plot of the lower order terms of B_x are given in Figure 12. Higher order terms become small as n increases due to scaling by $r^{-(n+1)}$. In equation (50) K_n is equal to zero when n is even. Hence B_x values for even terms are also zero.

A plot of the B_x, B_y, B_z, and total B are given in Figures 13, 14, 15, and 16 respectively. The analytical and finite element analysis solutions are approximately equal. The root-mean-squared errors are $B_x = 3.59 \times 10^{-4}$nT, $B_y = 2.03 \times 10^{-4}$nT, $B_z = 8.89 \times 10^{-4}$nT, and $B_{total} = 6.14 \times 10^{-4}$nT.

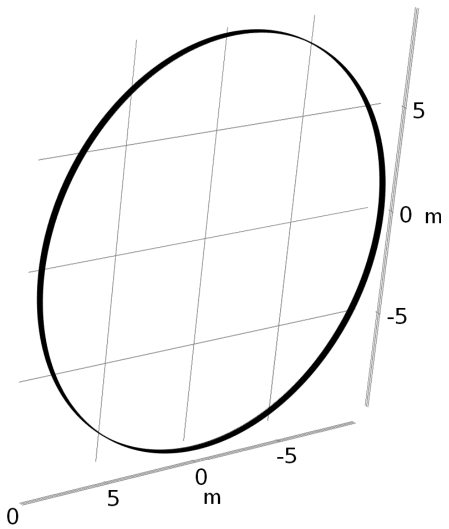

(i) Current band mesh

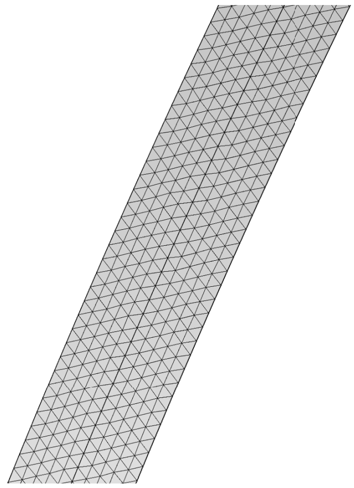

(ii) Close-up of current band mesh

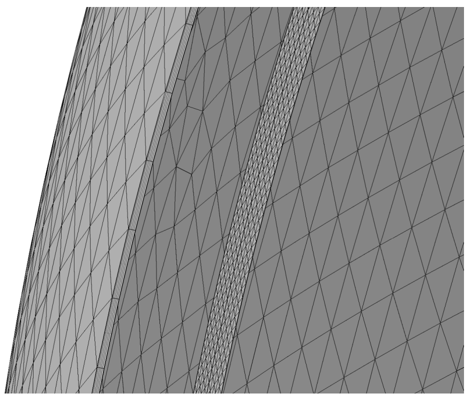

(iii) Meshed current band within a meshed spherical shell.

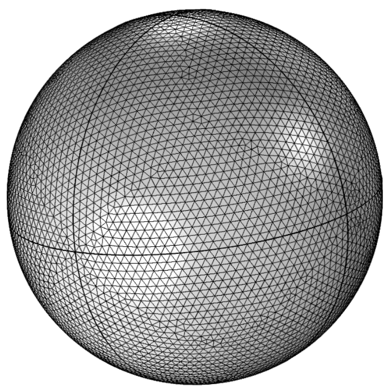

(iv) Fine mesh on shell surface

Figure 11: Finite element analysis model created in COMSOL of a permeable spherical shell with an internal current band.

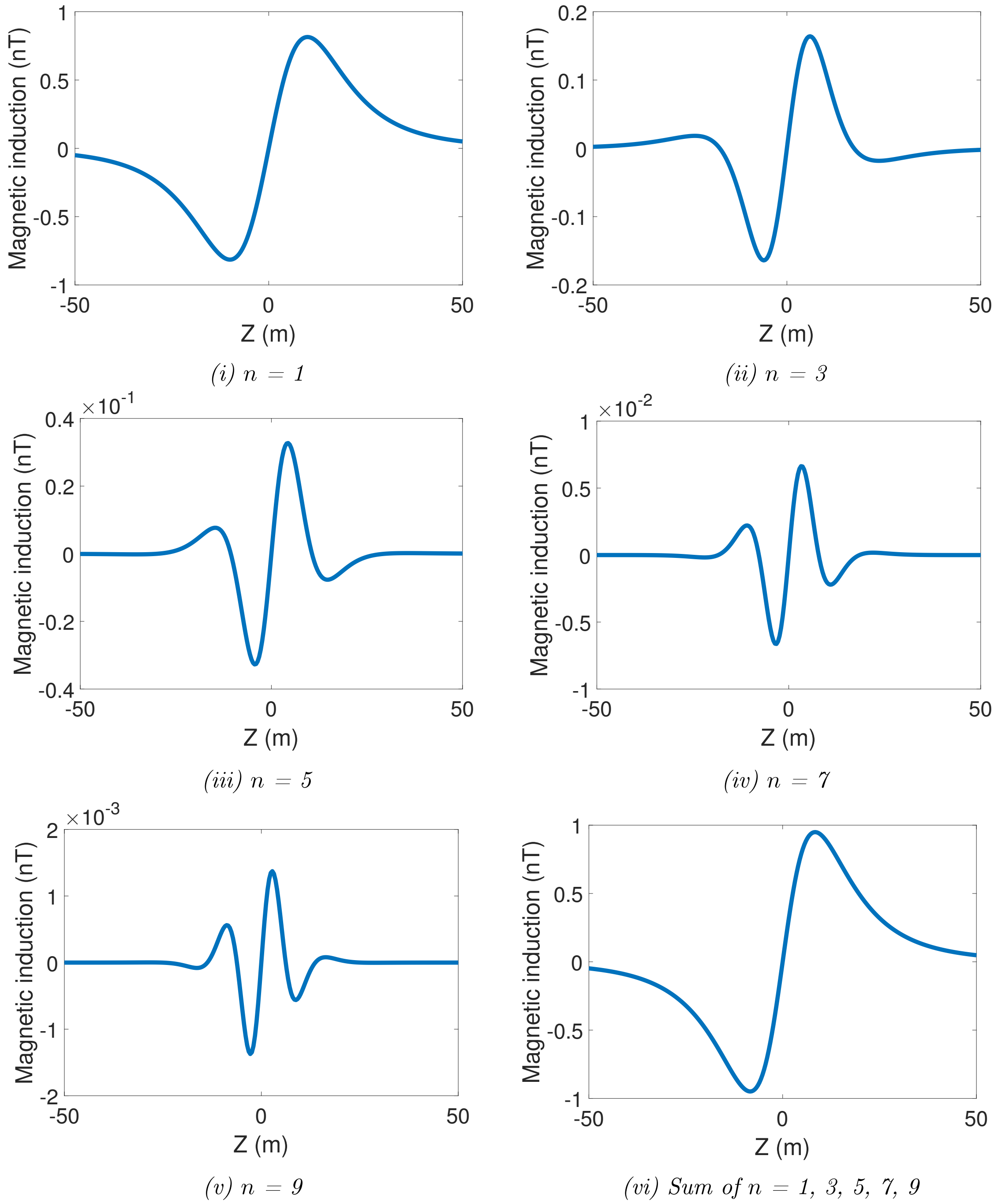

Figure 12: Lower order solutions of the magnetic induction B_x (nT) of a spherical shell with an internal current band where n denotes the order, $x = 20m$, $y = 0m$, $R_1 = 9.68m$, $R_2 = 9.98m$, $R_3 = 10m$, $J = 1Am^{-1}$, $\alpha = 1°$, $\mu_1 = 4\pi\times10^{-7}Hm^{-1}$, and $\mu_2/\mu_1 = 80$.

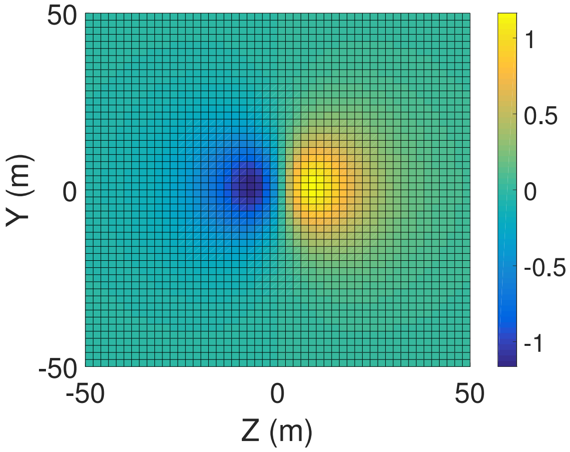

(i) *Analytical solution.*

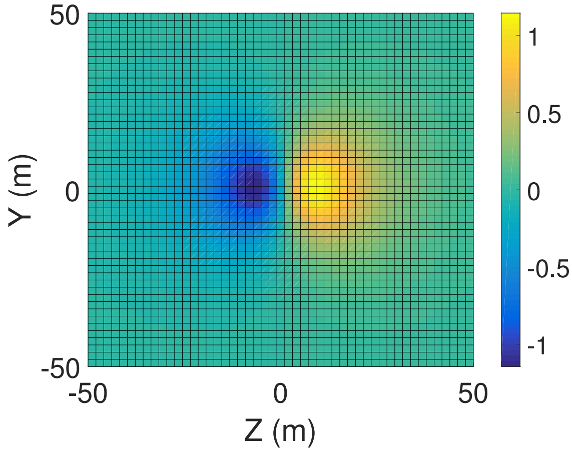

(ii) *FEA solution.*

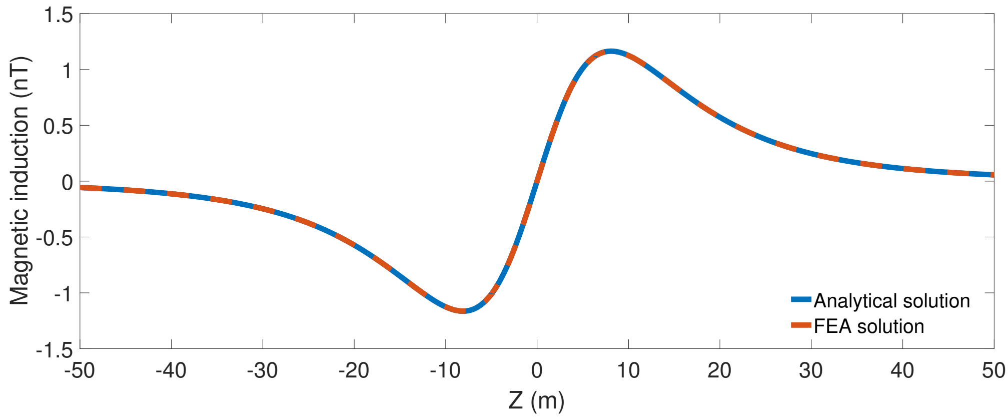

(iii) *Comparison between analytical and finite element analysis solutions where $y = 0m$.*

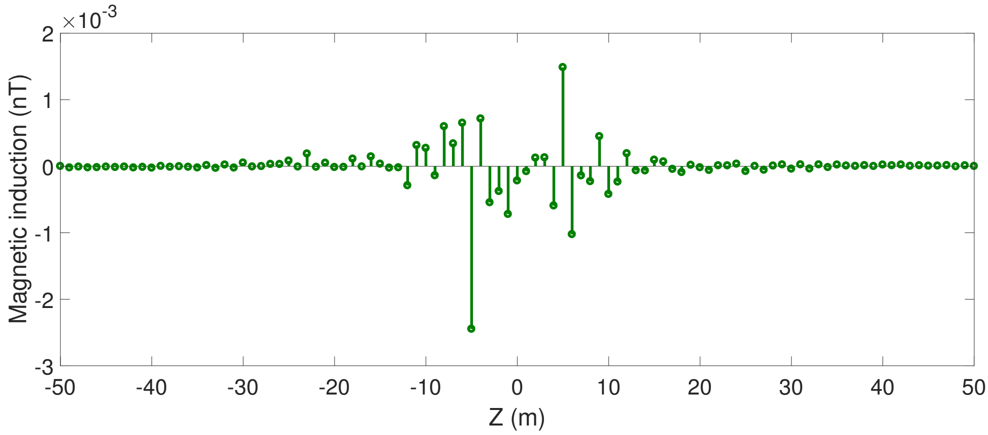

(iv) *Error between analytical and finite element analysis solutions where $y = 0m$.*

Figure 13: Magnetic induction B_x (nT) of a spherical shell with an internal current band in the y-z plane where $x = 20m$, $R_1 = 9.68m$, $R_2 = 9.98m$, $R_3 = 10m$, $J = 1Am^{-1}$, $\alpha = 1°$, $\mu_1 = 4\pi\times10^{-7}Hm^{-1}$, and $\mu_2/\mu_1 = 80$.

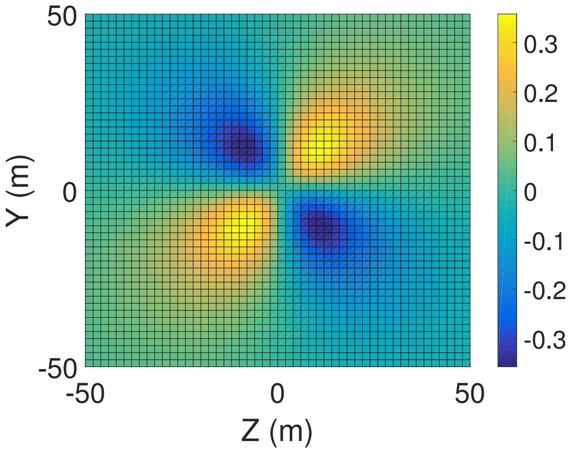

(i) Analytical solution.

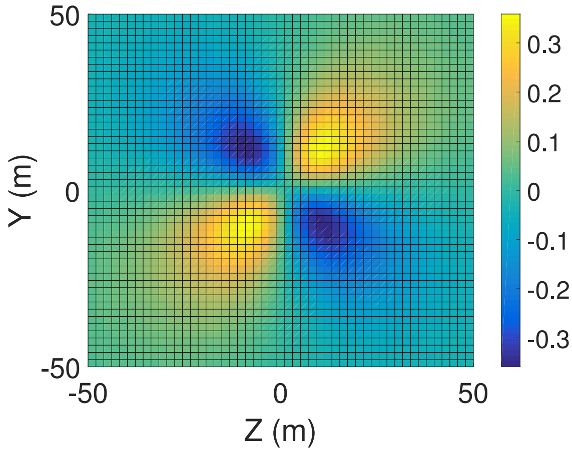

(ii) FEA solution.

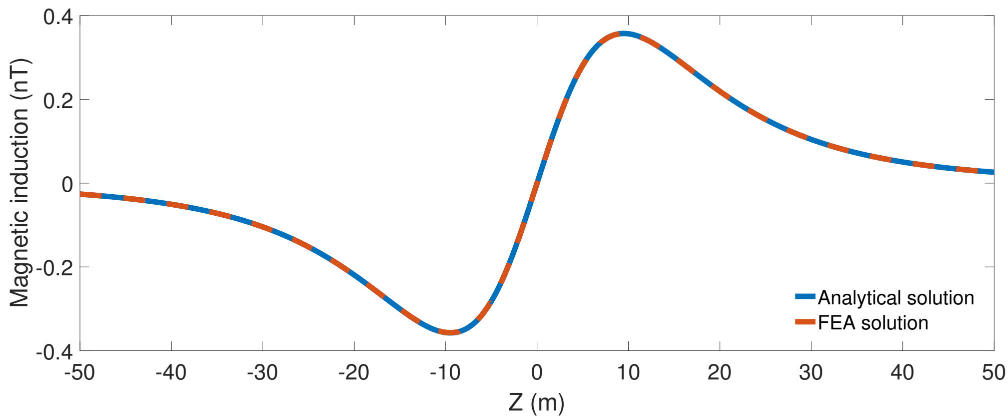

(iii) Comparison between analytical and finite element analysis solutions where $y = 10m$.

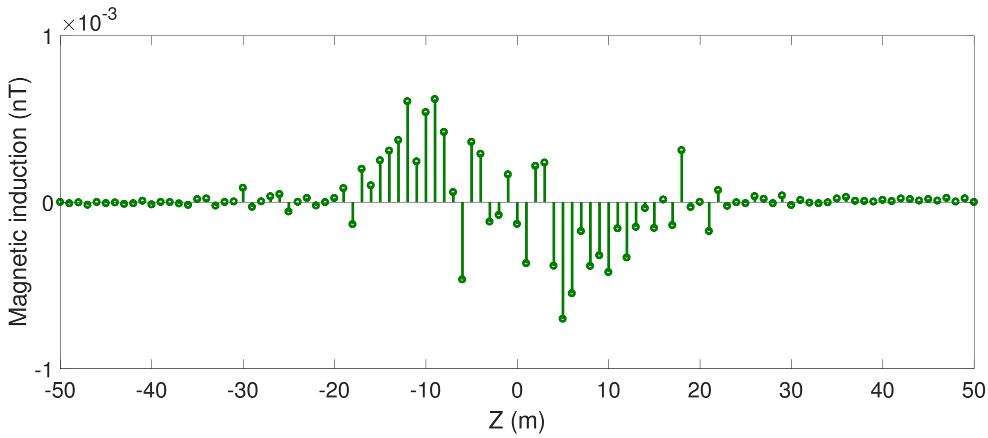

(iv) Error between analytical and finite element analysis solutions where $y = 10m$.

Figure 14: Magnetic induction B_y (nT) of a spherical shell with an internal current band in the y-z plane where $x = 20m$, $R_1 = 9.68m$, $R_2 = 9.98m$, $R_3 = 10m$, $J = 1Am^{-1}$, $\alpha = 1°$, $\mu_1 = 4\pi{\times}10^{-7}Hm^{-1}$, and $\mu_2/\mu_1 = 80$.

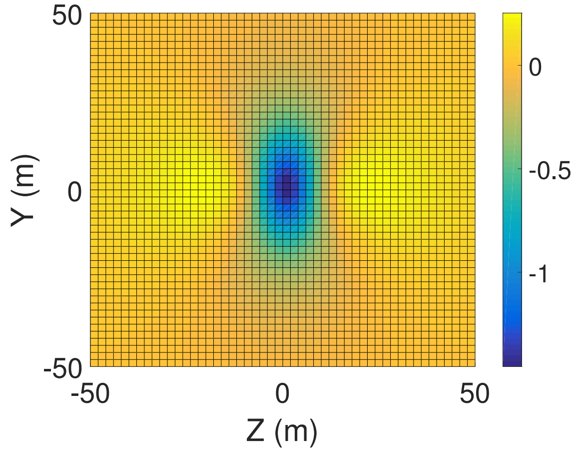

(i) Analytical solution.

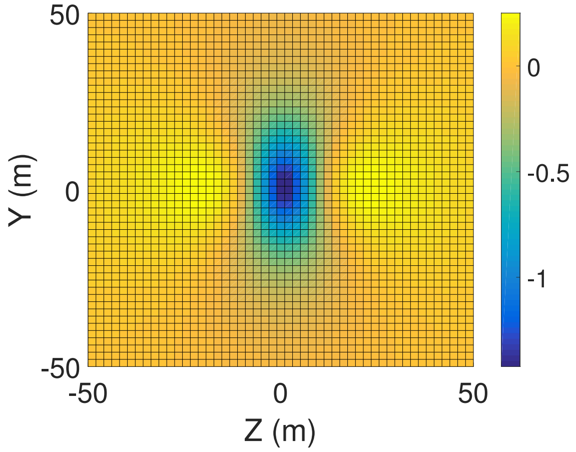

(ii) FEA solution.

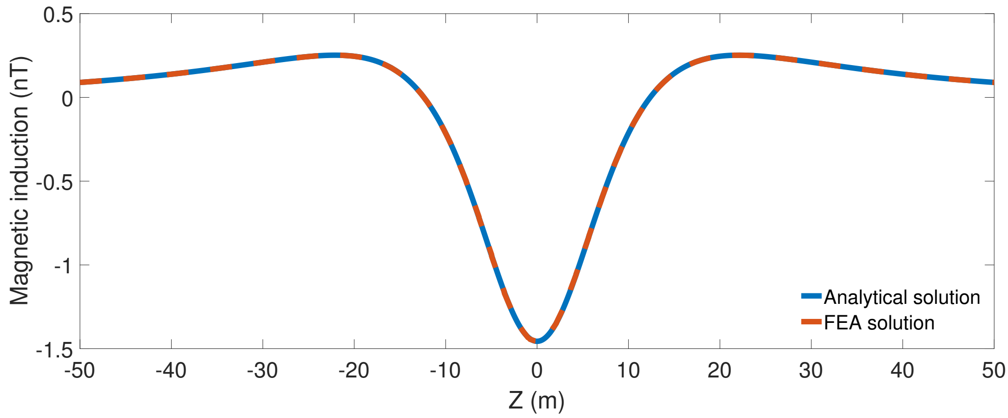

(iii) Comparison between analytical and finite element analysis solutions where y = 0m.

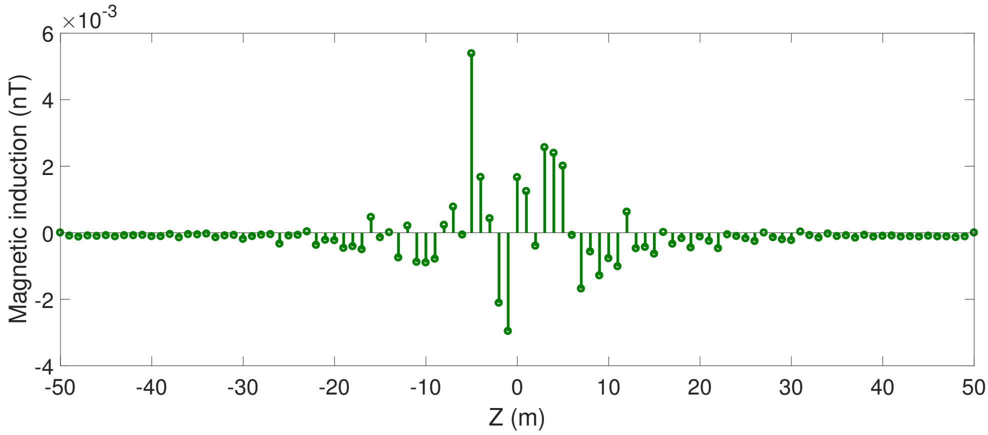

(iv) Error between analytical and finite element analysis solutions where y = 0m.

Figure 15: Magnetic induction B_z (nT) of a spherical shell with an internal current band in the y-z plane where x = 20m, $R_1 = 9.68m$, $R_2 = 9.98m$, $R_3 = 10m$, $J = 1Am^{-1}$, $\alpha = 1°$, $\mu_1 = 4\pi{\times}10^{-7}Hm^{-1}$, and μ_2/μ_1 = 80.

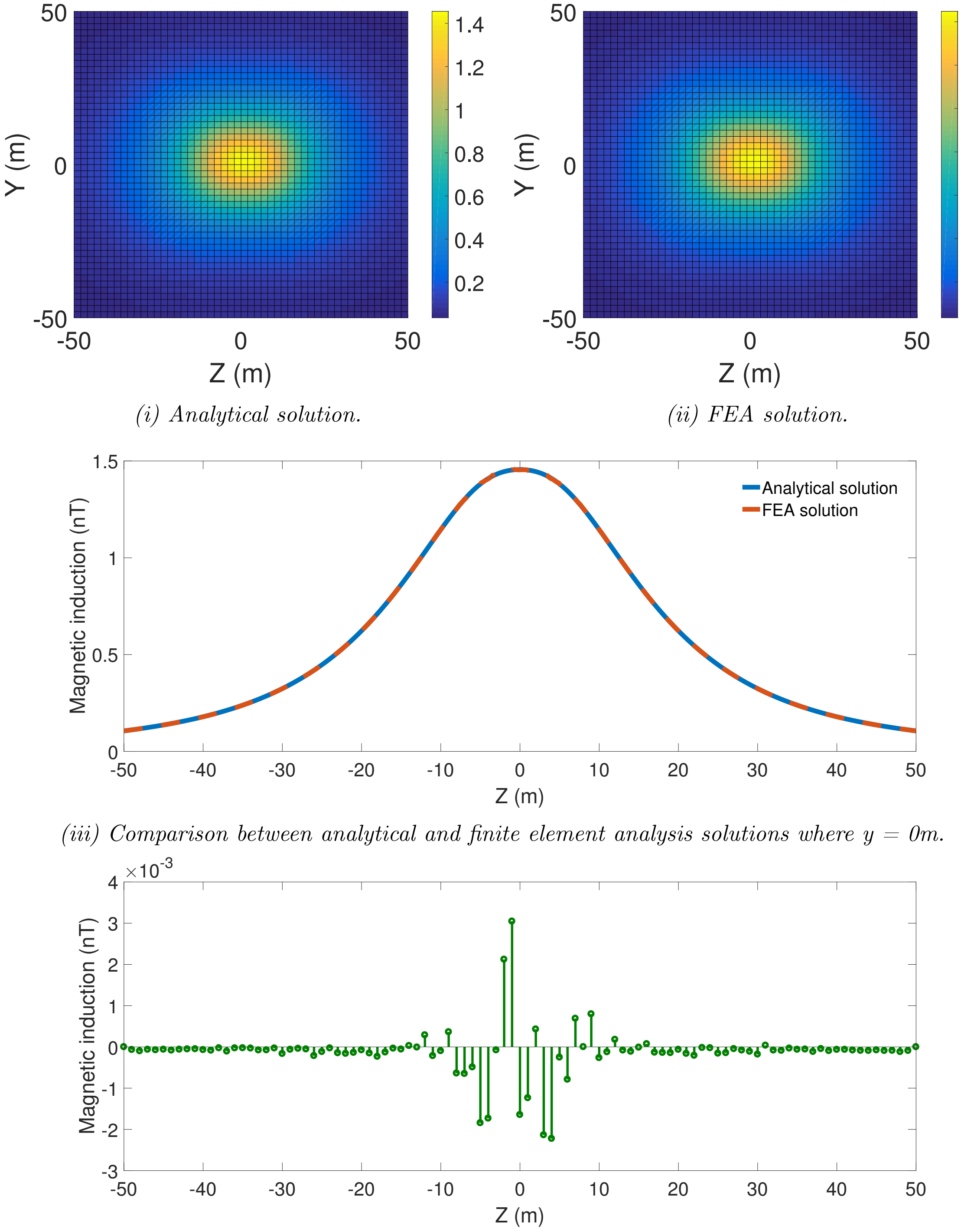

(i) Analytical solution.

(ii) FEA solution.

(iii) Comparison between analytical and finite element analysis solutions where $y = 0m$.

(iv) Error between analytical and finite element analysis solutions where $y = 0m$.

Figure 16: Magnetic induction B_{total} (nT) of a spherical shell with an internal current band in the y-z plane where $x = 20m$, $R_1 = 9.68m$, $R_2 = 9.98m$, $R_3 = 10m$, $J = 1Am^{-1}$, $\alpha = 1°$, $\mu_1 = 4\pi \times 10^{-7} Hm^{-1}$, and $\mu_2/\mu_1 = 80$.

6. Magnetic induction of a permeable spherical shell with an internal current band in uniform magnetic induction B_0

Consider the spherical shell with an internal current band in a background magnetic induction B_0 given in Figure 17.

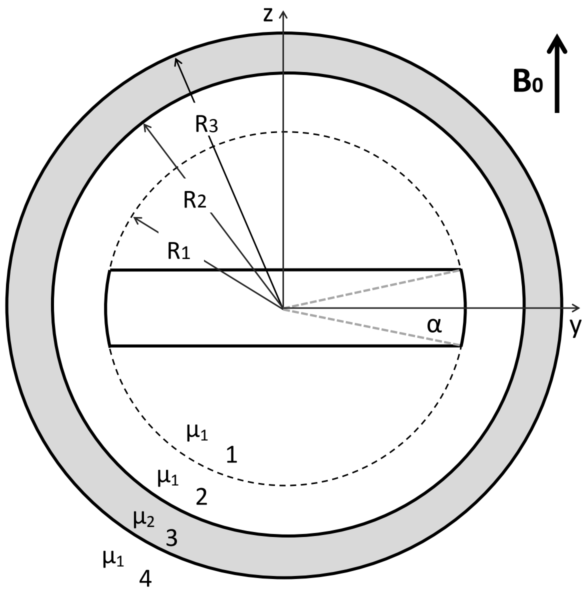

Figure 17: Spherical shell with an internal current band in uniform magnetic induction B_0 where R_1 is the current band radius, R_2 is the inner shell radius, R_3 is the outer shell radius, μ_1 and μ_2 are permeabilities, α is the angle of the current band considered from the centre of the spherical shell, and 1, 2, 3, and 4 are the regions considered.

6.1. Analytical solution

The analytical solution is found, thanks to the superposition principle, by adding the magnetic induction of the spherical shell in uniform magnetic induction B_0 to the magnetic induction of the current band in a spherical shell [2]. The final equations are given by:

$$B_r = \frac{H_0 \cos\theta}{\mu_1} + \frac{2D}{\mu_1 r^3}\cos\theta + \frac{1}{r\sin\theta}\sum_{p=1}^{\infty}\frac{F_p}{r^{p+1}}\frac{\partial}{\partial\theta}(\sin\theta P_p^1(\cos\theta)) \tag{55}$$

$$B_\theta = -\frac{H_0 \sin\theta}{\mu_1} + \frac{D}{\mu_1 r^3}\cos\theta + \frac{1}{r}\sum_{p=1}^{\infty} F_p P_p^1(\cos\theta)\frac{p}{r^{p+1}} \tag{56}$$

$$B_\phi = 0 \tag{57}$$

The spherical to rectangular vector transformations are given by equations (54a) - (54c).

6.2. Finite element analysis solution

The finite element analysis model was created using COMSOL version 5.3 [10] and the AC/DC Module [11]. The model uses the same model given in Figure 11 with the addition of a uniform magnetic field applied outside the spherical shell.

6.3. Comparison between analytical and finite element analysis solutions

A plot of the B_x, B_y, B_z, and B_{total} are given in Figures 18, 19, 20, 21 respectively. The analytical and finite element analysis solutions are approximately equal. The root-mean-squared errors are $B_x = 0.20$nT, $B_y = 0.04$nT, $B_z = 0.08$nT, and $B_{total} = 0.18$nT.

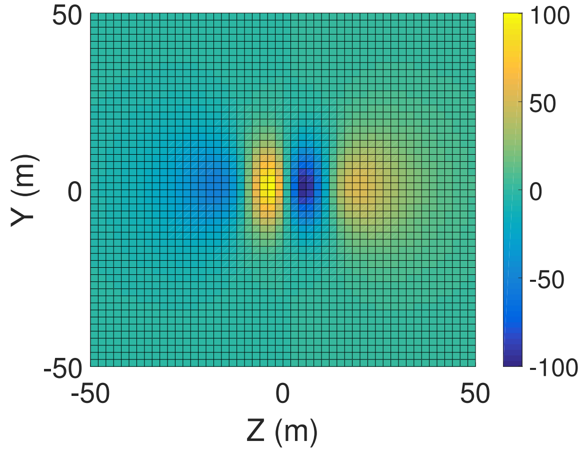

(i) Analytical solution.

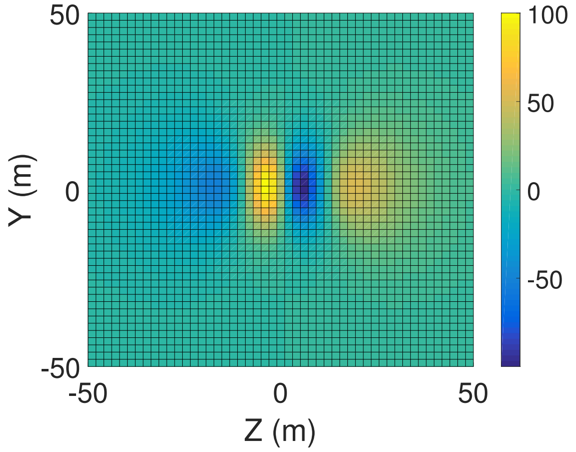

(ii) FEA solution.

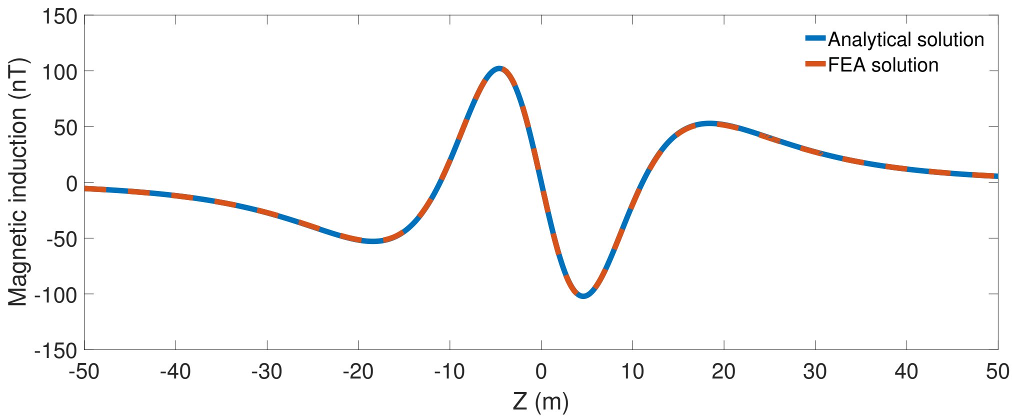

(iii) Comparison between analytical and finite element analysis solutions where $y = 0m$.

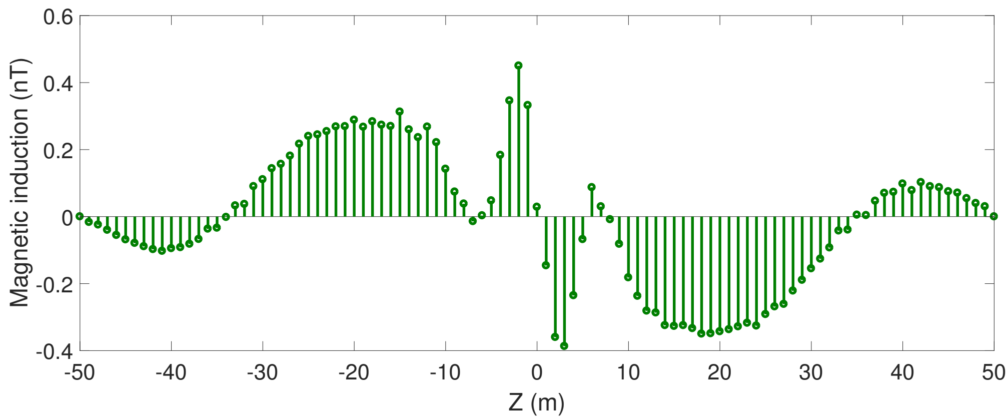

(iv) Error between analytical and finite element analysis solutions where $y = 0m$.

Figure 18: Magnetic induction B_x (nT) of a spherical shell with an internal current band in uniform magnetic induction in the y-z plane where $x = 20m$, $R_1 = 9.68m$, $R_2 = 9.98m$, $R_3 = 10m$, $J = -520Am^{-1}$, $B_0 = 55{,}000nT$, $\alpha = 1°$, $\mu_1 = 4\pi \times 10^{-7}Hm^{-1}$, and $\mu_2/\mu_1 = 80$.

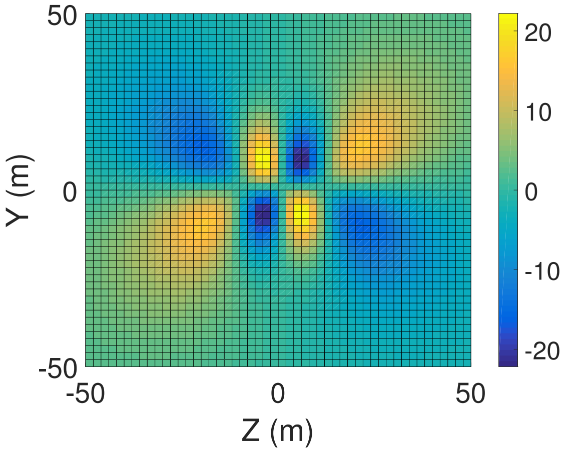

(i) Analytical solution.

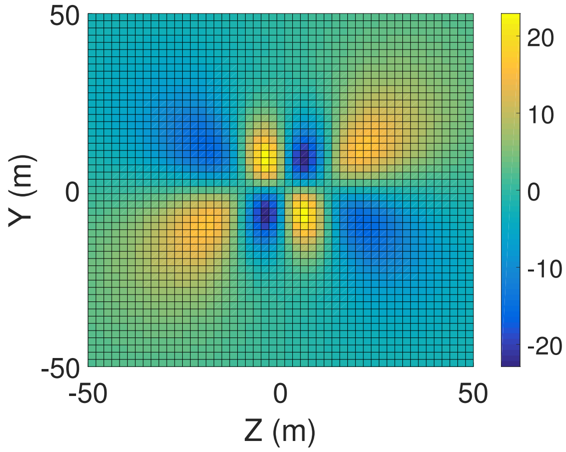

(ii) FEA solution.

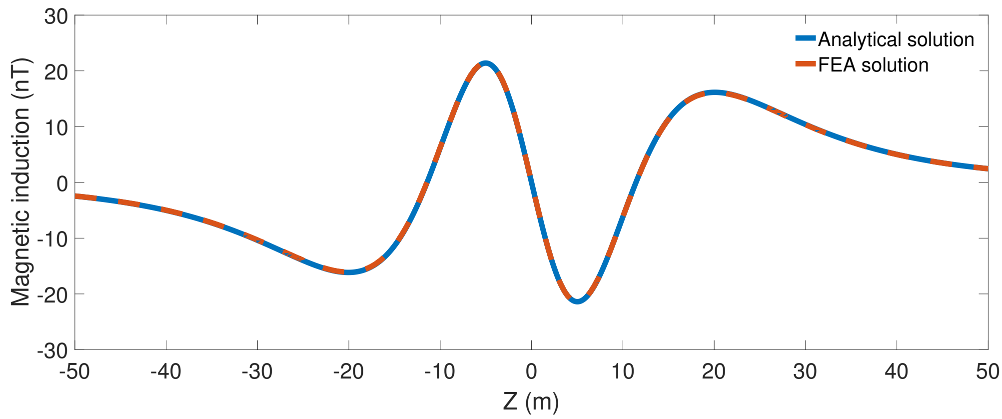

(iii) Comparison between analytical and finite element analysis solutions where $y = 10m$.

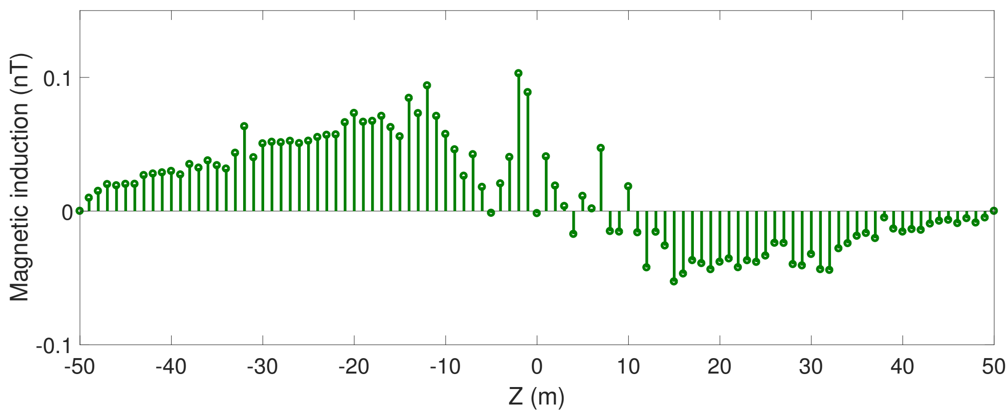

(iv) Error between analytical and finite element analysis solutions where $y = 10m$.

Figure 19: Magnetic induction B_y (nT) of a spherical shell with an internal current band in uniform magnetic induction in the y-z plane where $x = 20m$, $R_1 = 9.68m$, $R_2 = 9.98m$, $R_3 = 10m$, $J = -520Am^{-1}$, $B_0 = 55,000nT$, $\alpha = 1°$, $\mu_1 = 4\pi\times10^{-7}Hm^{-1}$, and $\mu_2/\mu_1 = 80$.

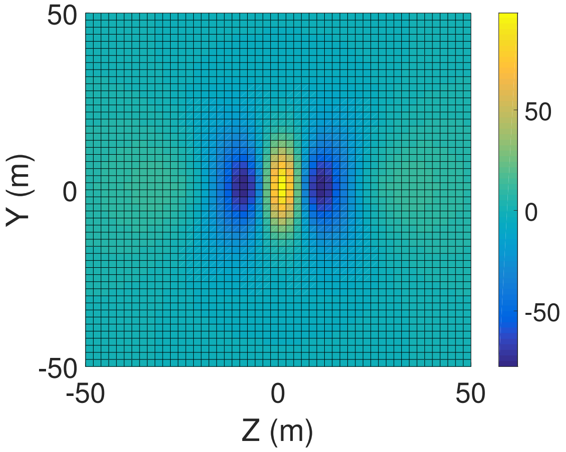

(i) Analytical solution.

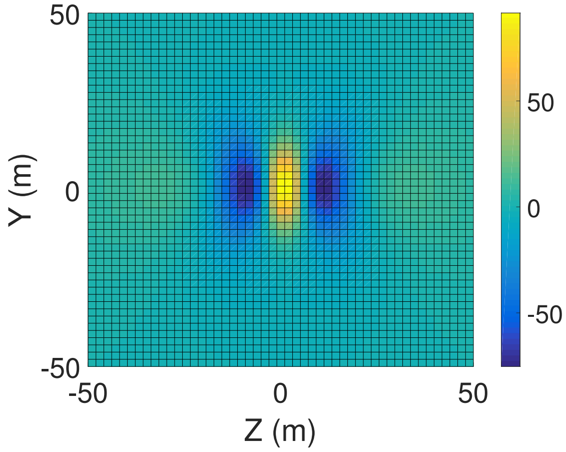

(ii) FEA solution.

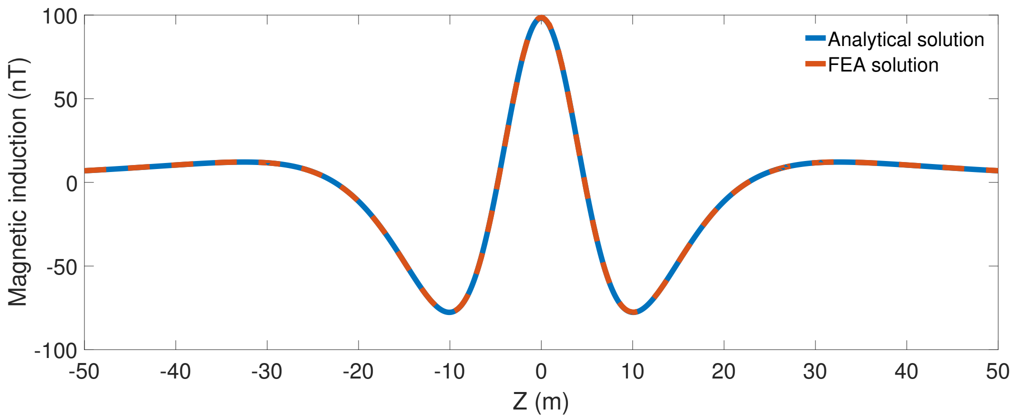

(iii) Comparison between analytical and finite element analysis solutions where y = 0m.

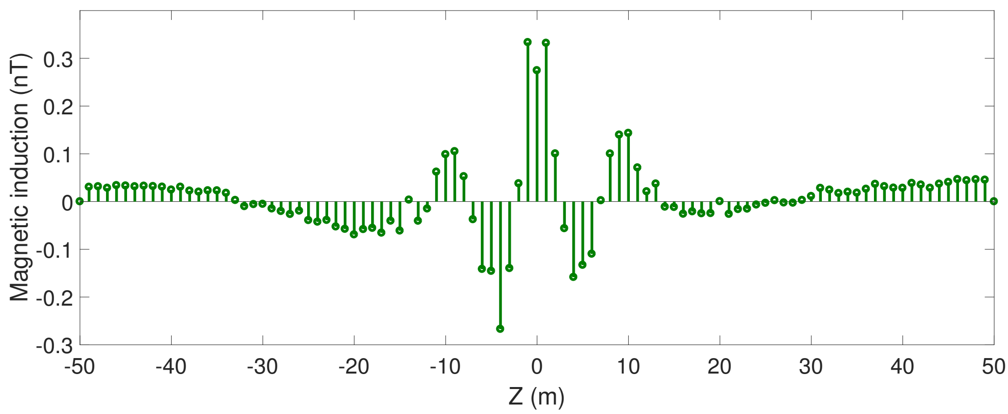

(iv) Error between analytical and finite element analysis solutions where y = 0m.

Figure 20: Magnetic induction B_z (nT) of a spherical shell with an internal current band in uniform magnetic induction in the y-z plane where x = 20m, $R_1 = 9.68m$, $R_2 = 9.98m$, $R_3 = 10m$, $J = -520Am^{-1}$, $B_0 = 55,000nT$, $\alpha = 1°$, $\mu_1 = 4\pi \times 10^{-7} Hm^{-1}$, and μ_2/μ_1 = 80.

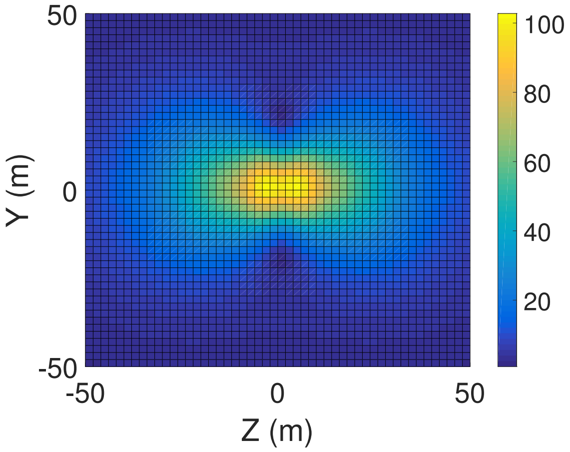

(i) Analytical solution.

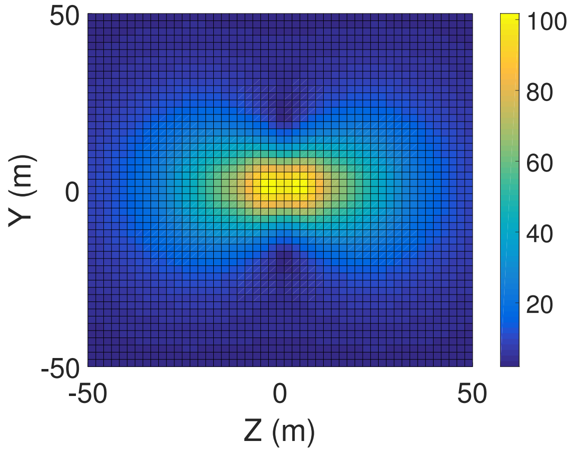

(ii) FEA solution.

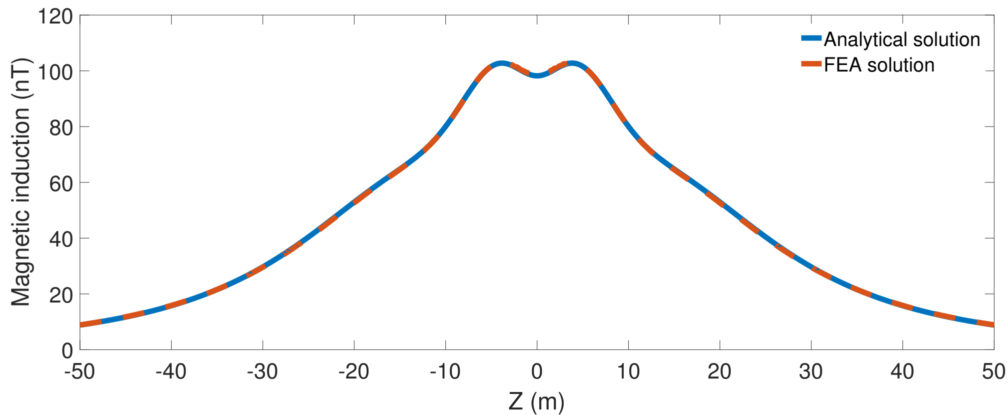

(iii) Comparison between analytical and finite element analysis solutions where y = 0m.

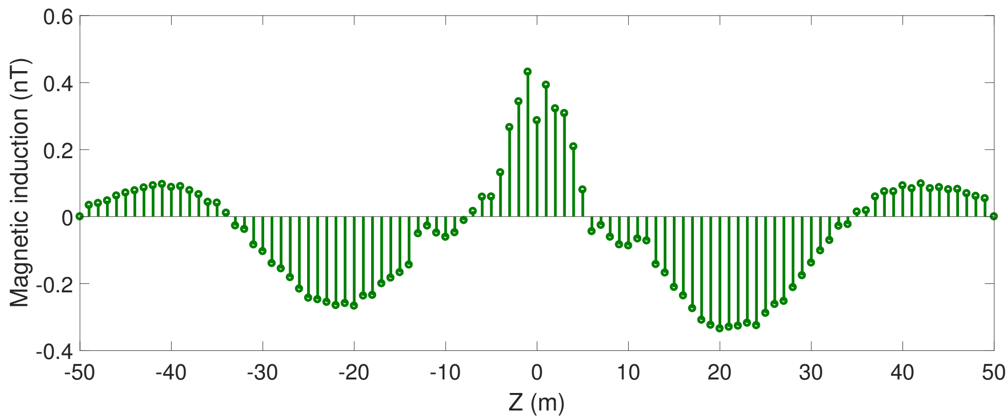

(iv) Error between analytical and finite element analysis solutions where y = 0m.

Figure 21: Magnetic induction B_{total} (nT) of a spherical shell with an internal current band in uniform magnetic induction in the y-z plane where x = 20m, $R_1 = 9.68m$, $R_2 = 9.98m$, $R_3 = 10m$, $J = -520Am^{-1}$, $B_0 = 55,000nT$, $\alpha = 1°$, $\mu_1 = 4\pi{\times}10^{-7}Hm^{-1}$, and μ_2/μ_1 = 80.

7. Conclusions

In this report we compared analytical and finite element solutions to validate the use of COMSOL software for calculating the magnetic signature of permeable materials with internal current bands in background magnetic fields.

Importantly, the analytical solutions were in close agreement with the finite element analysis solutions for the magnetic induction of a permeable spherical shell with an internal current band in uniform magnetic induction B_0 for x, y, z axes, and the total field.

Based on the results presented in this report, COMSOL may be used to calculate the magnetic induction of permeable materials with internal current bands in background magnetic fields.

8. Further work

This work considered magnetic induction of a permeable *spherical* shell with an internal current band in a uniform magnetic induction. Further work should consider the magnetic induction of a permeable *prolate spheroidal* shell with an internal current band in a uniform magnetic induction to better model a submarine.

This work may be used to study the *induced* magnetic signature of a submarine in a background magnetic field. Future work should focus on accurately modelling the *permanent* magnetic signature, and stress magnetisation, of a submarine using COMSOL.

9. Acknowledgements

Thank you to Adam Fairley for his advice regarding COMSOL modelling of the spherical shell. Thank you to Justin Dinale, Mark Hallett, and Mark Readhead for reviewing this report and making valuable suggestions for improvement.

10. References

[1] S. H. Brown and F. E. Baker Jr, 'Magnetic induction of ferromagnetic spherical bodies and current bands', *Journal of Applied Physics*, vol. 53, no. 6, pp. 3981–3990, 1982.

[2] F. E. Baker Jr and S. H. Brown, 'Magnetic induction of spherical and prolate spheroidal bodies with infinitesimally thin current bands having a common axis of symmetry and in a uniform inducing field. A summary', David W. Taylor Naval Ship Research and Development Centre Bethesda MD, Tech. Rep., 1982.

[3] F. Baker, S. Brown, J. Brauer and T. Gerhardt, 'Comparison of magnetic fields computed by finite element and classical series methods', *International Journal for Numerical Methods in Engineering*, vol. 19, no. 2, pp. 271–280, 1983.

[4] P. M. Morse and H. Feshbach, *Methods of Theoretical Physics*. Mc Graw-Hill Book Company, 1953.

[5] J. J. Holmes, 'Modeling a ship's ferromagnetic signatures', *Synthesis Lectures on Computational Electromagnetics*, vol. 2, no. 1, pp. 1–75, 2007.

[6] P. Moon and D. E. Spencer, *Field theory handbook: including coordinate systems, differential equations and their solutions*. Springer, 2012.

[7] M. Abramowitz and I. A. Stegun, *Handbook of mathematical functions*. Dover Publications, New York, 1965.

[8] A. C. Polycarpou, 'Introduction to the finite element method in electromagnetics', *Synthesis Lectures on Computational Electromagnetics*, vol. 1, no. 1, pp. 1–126, 2005.

[9] J. D. Jackson, *Classical electrodynamics*. Wiley, 1999.

[10] *COMSOL multiphysics reference manual version 5.3*, version 5.3, COMSOL AB, www.comsol.com, 2018.

[11] *AC/DC module user's guide*, version 5.3, COMSOL AB, www.comsol.com, 2018.

This page is intentionally blank

DEFENCE SCIENCE AND TECHNOLOGY GROUP DOCUMENT CONTROL DATA				1. DLM/CAVEAT (OF DOCUMENT)

2. TITLE	3. SECURITY CLASSIFICATION (FOR UNCLASSIFIED LIMITED RELEASE USE (L) NEXT TO DOCUMENT CLASSIFICATION)
Magnetic signatures of spherical bodies in Earth's magnetic field — a comparison of analytical and finite element analysis solutions	Document (U) Title (U) Abstract (U)
4. AUTHOR	5. CORPORATE AUTHOR
Ryan Michael Thomas	Defence Science and Technology Group Locked Bag 7005, Liverpool, NSW 1871, Australia

6a. DST GROUP NUMBER	6b. AR NUMBER	6c. TYPE OF REPORT	7. DOCUMENT DATE
DST-Group–TR–3530	AR-017-281	Technical Report	September, 2018

8. OBJECTIVE ID	9. TASK NUMBER	10. TASK SPONSOR
	17/525	SEA 1000

11. MSTC	12. STC
Maritime Autonomy	Magnetics & Payload Sensors
13. DOWNGRADING/DELIMITING INSTRUCTIONS	14. RELEASE AUTHORITY
	Chief, Maritime Division

15. SECONDARY RELEASE STATEMENT OF THIS DOCUMENT

Approved for Public Release

OVERSEAS ENQUIRIES OUTSIDE STATED LIMITATIONS SHOULD BE REFERRED THROUGH DOCUMENT EXCHANGE, PO BOX 1500, EDINBURGH, SA 5111

16. DELIBERATE ANNOUNCEMENT

No Limitations

17. CITATION IN OTHER DOCUMENTS

No Limitations

18. RESEARCH LIBRARY THESAURUS

Magnetic signature, magnetic induction, spherical shell

19. ABSTRACT

Calculating magnetic signatures using analytical techniques becomes infeasible for complex geometries such as submarines, hence numerical techniques, such as finite element analysis, must be used instead. In this report we compare analytical and finite element solutions utilising COMSOL for calculating the magnetic induction of a permeable spherical shell with an internal current band in uniform magnetic induction. The analytical and finite element analysis solutions were found to be approximately equal, this verifies that modelling of magnetic signatures of submarines using COMSOL will generate correct data.